

LA-9060-PR

Progress Report

C.2

CIC-14 REPORT COLLECTION
REPRODUCTION
COPY

Los Alamos National Laboratory is operated by the University of California for the United States Department of Energy under contract W-7405-ENG-36.

*Applied Nuclear Data
Research and Development*

April 1 - June 30, 1981

LOS ALAMOS NATL. LAB. LIBS.
3 9338 00312 2107



Los Alamos Los Alamos National Laboratory
Los Alamos, New Mexico 87545

The four most recent reports in this series, unclassified, are LA-8524-PR, LA-8630-PR, LA-8757-PR, and LA-8874-PR.

This work was performed under the auspices of the US Department of Energy's Division of Reactor Research and Technology, Office of Basic Energy Sciences, and Office of Fusion Energy; the Spent Fuel Project Office under the technical direction of the Savannah River Laboratory; and the Electric Power Research Institute.

DISCLAIMER

This report was prepared as an account of work sponsored by an agency of the United States Government. Neither the United States Government nor any agency thereof, nor any of their employees, makes any warranty, express or implied, or assumes any legal liability or responsibility for the accuracy, completeness, or usefulness of any information, apparatus, product, or process disclosed, or represents that its use would not infringe privately owned rights. References herein to any specific commercial product, process, or service by trade name, trademark, manufacturer, or otherwise, does not necessarily constitute or imply its endorsement, recommendation, or favoring by the United States Government or any agency thereof. The views and opinions of authors expressed herein do not necessarily state or reflect those of the United States Government or any agency thereof.

Applied Nuclear Data Research and Development

April 1—June 30, 1981

Compiled by
P. G. Young



CONTENTS

I.	THEORY AND EVALUATION OF NUCLEAR CROSS SECTIONS	
A.	R-Matrix Analysis of $p^{-28}\text{Si}$ Scattering	1
B.	Verification of Parameters Needed for $^{87,88}\text{Y} + n$ Calculations.....	4
C.	Deformed Optical Model Analysis of $n + ^{169}\text{Tm}$ Reactions.....	6
D.	Statistical Model Calculations of the $^{169}\text{Tm}(n, \gamma) ^{170}\text{Tm}$ Cross Section.	8
E.	Statistical Model Calculations of Neutron Reactions on ^{239}Pu between 0.01 and 5 MeV.....	12
F.	New Fission Neutron Spectrum Representation for Evaluated Nuclear Data Files.....	15
G.	Calculation of Excited State Cross Sections for Actinide Nuclei.....	19
II.	NUCLEAR CROSS-SECTION PROCESSING AND TESTING	
A.	Los Alamos National Laboratory - Benchmark Calculations.....	20
B.	Processed Multigroup and Few-Group Cross Sections.....	20
C.	Integral Cross Sections in Three Representations of the ^{252}Cf Spontaneous Fission Spectrum.....	23
D.	NJOY Development.....	25
III.	FISSION PRODUCTS AND ACTINIDES: YIELDS, DECAY DATA, DEPLETION, AND BUILDUP	
A.	Comparisons of Aggregate ^{235}U and ^{239}Pu Fission-Product β^- and γ Decay Energies with Summation Calculations Based on Recent Libraries.....	35
B.	Integral Data Testing of ENDF/B Fission Product Data.....	43
C.	Neutron Capture Branching Fractions.....	46
D.	ENDF/B-V Reference Data Report.....	46
E.	Neutron Production in UO_2F_2 from the Spontaneous-Fission and Alpha Decay of U Nuclides and Subsequent $^{17,18}\text{O}(\alpha, n)$ and $^{19}\text{F}(\alpha, n)$ Reactions.....	50
	REFERENCES.....	52

APPLIED NUCLEAR DATA RESEARCH AND DEVELOPMENT
QUARTERLY PROGRESS REPORT
April 1 - June 30, 1981

Compiled by

P. G. Young

ABSTRACT

This progress report describes the activities of the Los Alamos Nuclear Data Group for April 1 through June 30, 1981. The topical content is summarized in the Table of Contents.

I. THEORY AND EVALUATION OF NUCLEAR CROSS SECTIONS

A. R-Matrix Analysis of p-²⁸Si Scattering [G. M. Hale and D. Hoyle (University of Washington)]

In the course of studying the giant Gamow-Teller resonance in the β^+ decay of moderately light nuclei, Adelberger's group at the University of Washington has made extensive cross section and analyzing power measurements for protons incident on several $Z = N$ targets. We are doing an R-matrix analysis of some of these data in order to check the J^π assignments for the resonances, using the general capabilities of the Energy Dependent Analysis.

The data comprise more than 7200 measurements of cross sections and analyzing powers for p-²⁸Si scattering at energies between 2.6 and 5.2 MeV. We have included 23 levels in this region, starting from resonance parameters found by Ikossi (U. of Washington) in fitting the same data. Examples of the preliminary fit are shown in Figs. 1 and 2 for cross sections and analyzing powers at 117°. Most of the structure in the measurements is accounted for by the levels included, but some questions remain concerning normalizations and the lack of agreement at energies around 5.1 MeV.

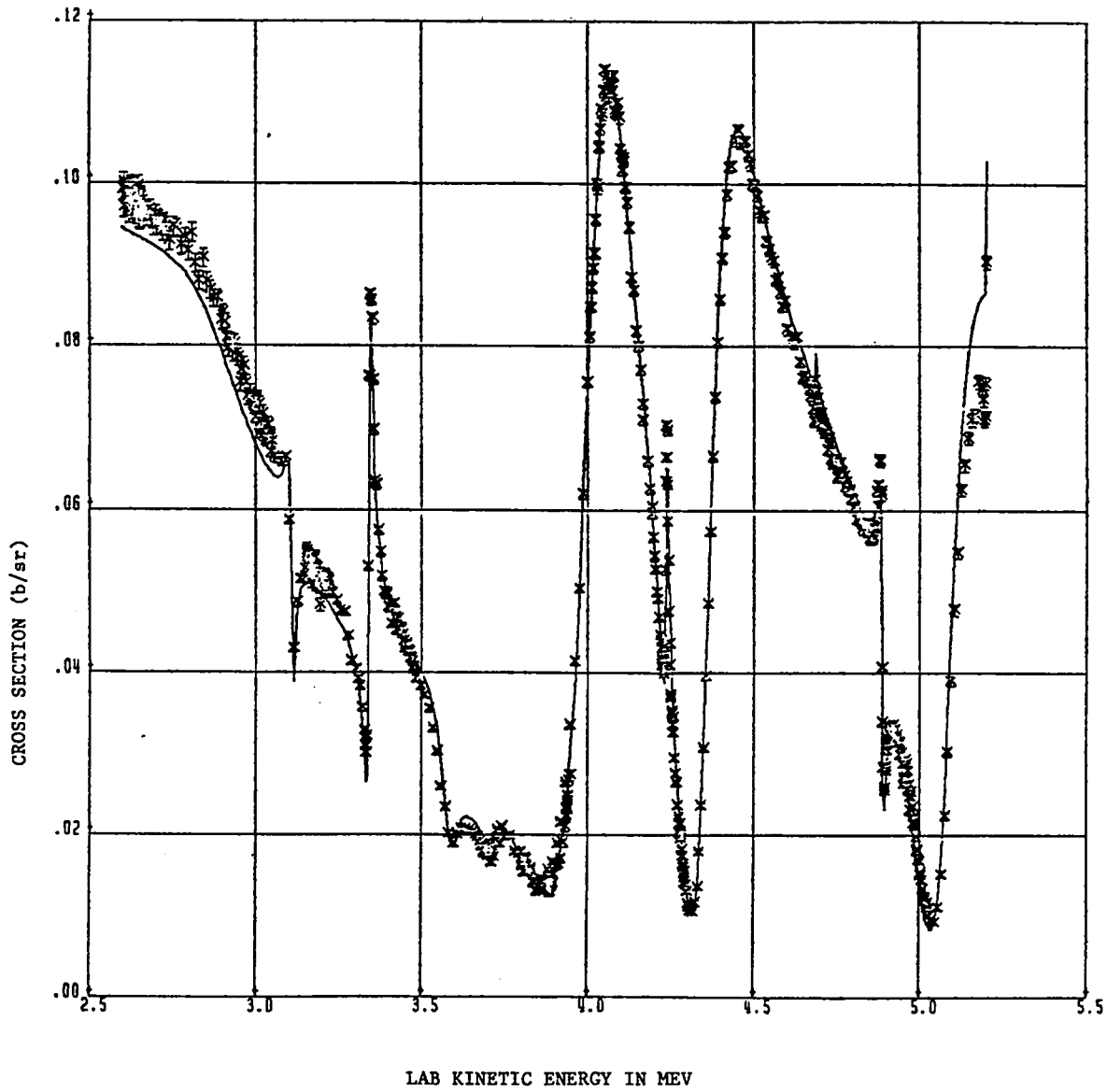


Fig. 1.

R-matrix fit (solid curve) to the cross-section excitation measured at 117° by the University of Washington group.

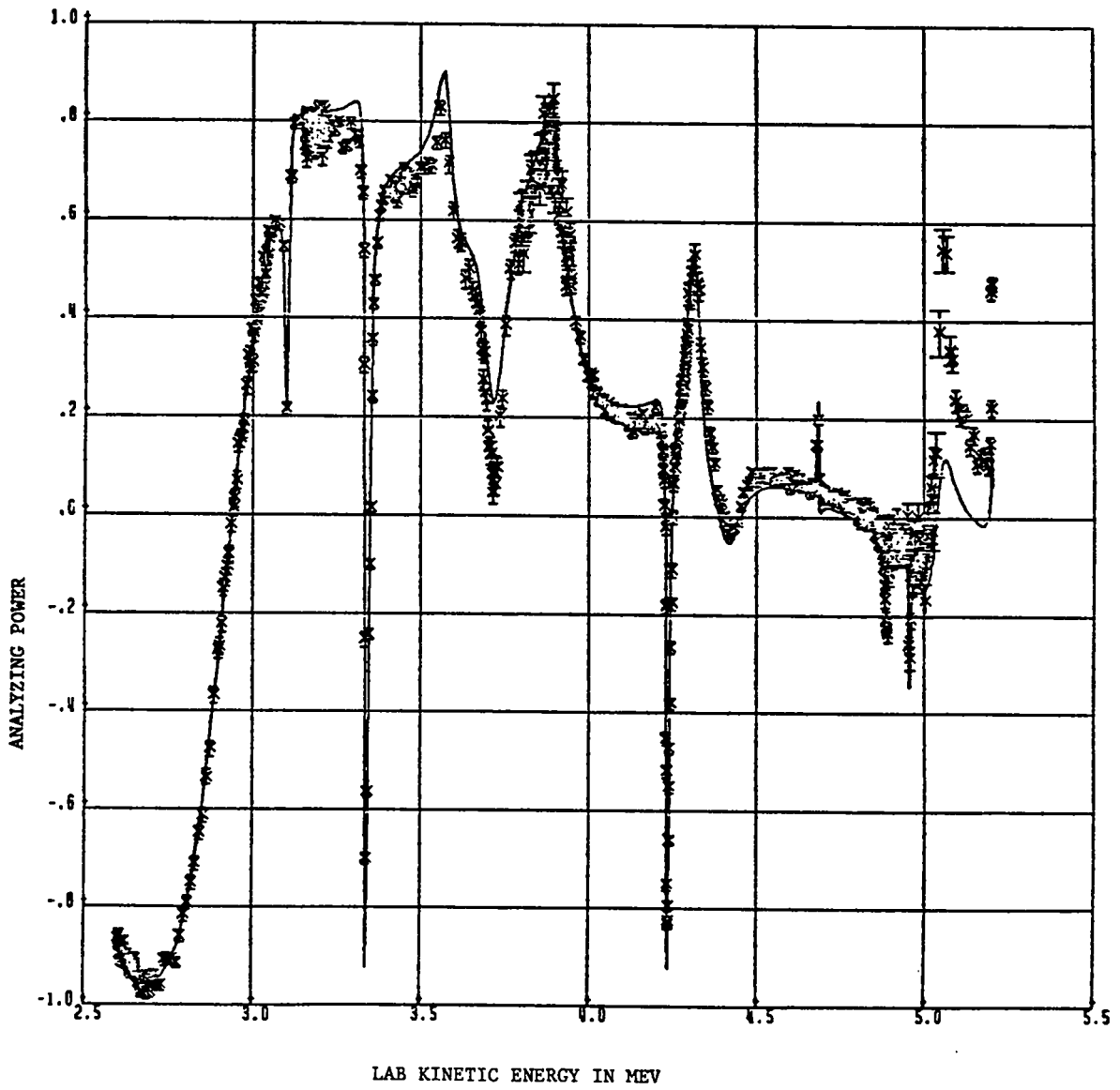


Fig. 2.

R-matrix fit (solid curve) to the analyzing-power excitation measured at 117° by the University of Washington group.

B. Verification of Parameters Needed for $^{87,88}\text{Y} + n$ Calculations (E. D. Arthur)

In our calculations¹ of neutron-induced reactions on proton-rich yttrium isotopes, an attempt was made to minimize effects arising from uncertainties in various input parameters through a consistent analysis of neutron experimental data available for several stable and unstable yttrium and zirconium isotopes. However, further information is still needed to reduce remaining unknowns occurring in calculational parameters for such unstable nuclei. For example, the calculated $^{87}\text{Y}(n, np + npn)$ cross section around threshold is extremely sensitive to ^{87}Y level density parameters and gamma-ray strength functions used in the calculation.

A possible independent source that may provide guidance for such parameters would be excitation functions measured for charged-particle reactions on strontium isotopes. The most suitable candidates would apparently be $^{87,88}\text{Sr}(p, xn)$ reactions. A literature search found measurements² only of $^{88}\text{Sr}(p, xn)$ cross sections, and these appear in error because measured (p, n) and $(p, n) + (p, 2n)$ sums often exceed plausible values³ for the total proton reaction cross section. Analysis of $^{86}\text{Sr}(d, xn)$ reactions are possible, but direct-reaction effects play an important role in the theoretical description. Also, no suitable published data exist. Finally, $^{85}\text{Rb}(\alpha, xn)$ reactions were considered but difficulties occur because such alpha-induced reactions lead to different spin distributions populated for the initial compound system over that obtained with neutrons or protons. Additionally the production of the $^{87,88}\text{Y}$ nuclei of interest occurs through $(\alpha, 2n)$ and $(\alpha, 3n)$ reactions at high energies, a situation that increases the difficulty of the calculations.

It appears from our literature search, therefore, that new measurements would be necessary to provide the level density information described above. Although $^{88}\text{Sr}(p, xn)$ and $^{87}\text{Sr}(p, xn)$ reactions appear to offer the best possibilities, calculations were made in which level density and gamma strengths were varied to test the sensitivity of the calculated results. The most sensitivity occurs for the $^{87}\text{Sr}(p, n)$ reaction as shown in Fig. 3. The change in this cross section appears to be related to variations in the calculated (p, np) cross section, which is strongly affected by the indicated parameter changes. On the other hand, little change occurs for the $^{87}\text{Sr}(p, 2n)$ cross section. Similar changes in $^{87,88}\text{Y}$ level density or strength functions produced little change in calculated $^{88}\text{Sr}(p, n)$ or $^{88}\text{Sr}(p, 2n)$ cross sections.

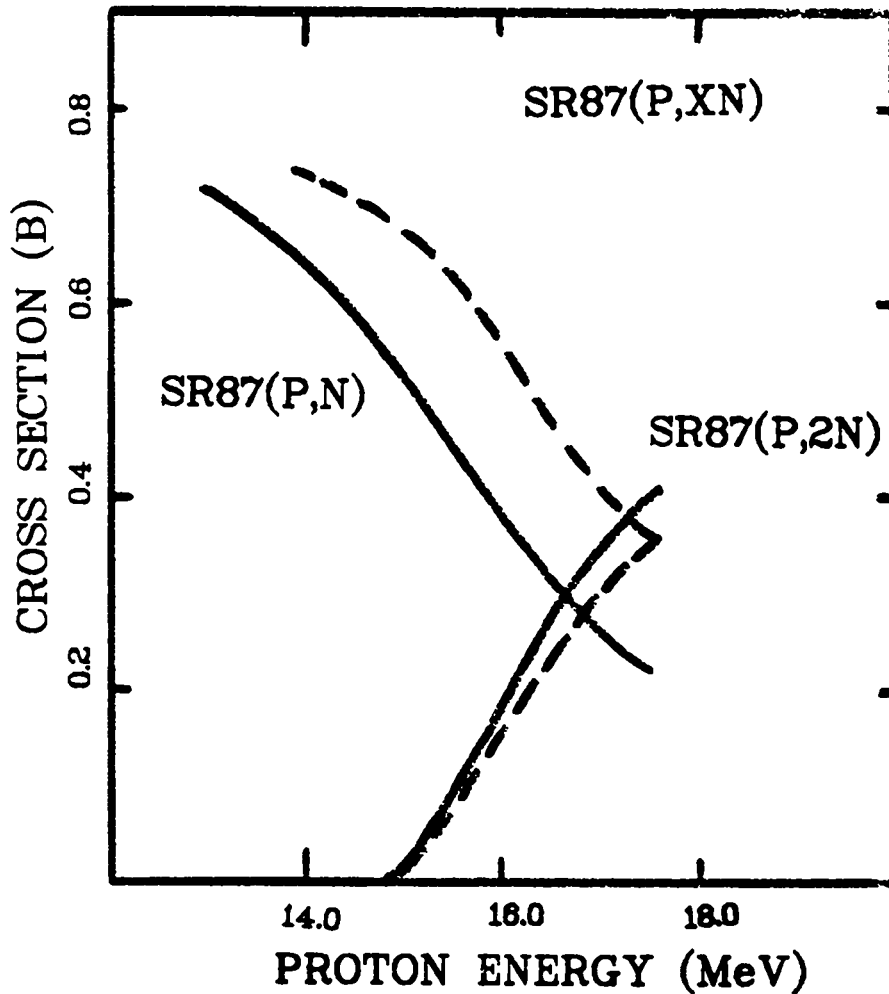


Fig. 3.

Variation of calculated $^{87}\text{Sr}(p,n)$ and $(p,2n)$ cross sections to changes in input parameter values. The solid curve represents cross sections calculated using the parameters of Ref. 1; the dashed curve occurs when the ^{87}Y level density is increased by approximately a factor of 2, coupled with a doubling of the gamma-ray strength function normalization.

Because the primary cause of the sensitivity of the $^{87}\text{Sr}(p,n)$ cross section to these parameter changes appears to result from their effect on the (p,np) reaction values, a more direct measure would be a determination of the $^{87}\text{Sr}(p,np + pn)$ cross section. Because this leads to the stable ^{86}Sr residual nucleus, radiochemical methods cannot be used. However, Fig. 4 shows the sensitivity of the calculated proton production spectrum resulting from 15 MeV $p + ^{87}\text{Sr}$ reactions to the indicated parameter changes. The lower energy portion of the spectrum results mainly from (p,np) reactions and shows greater than a factor of 2 change when the parameters are varied as shown. Since these low-energy protons are governed mainly by statistical processes, they should be symmetric about 90° , thus simplifying possible experimental measurements. Finally, the ^{87}Y compound system is reached in this reaction so that it represents a fairly direct simulation of the $^{87}\text{Y}(n,np)$ reaction.

C. Deformed Optical Model Analysis of $n + ^{169}\text{Tm}$ Reactions (E. D. Arthur)

A preliminary set of deformed optical model parameters was derived as an initial step in a complete analysis of $n + ^{169}\text{Tm}$ reactions. Because ^{169}Tm is strongly deformed, it is physically more valid to employ deformed optical-model calculations for neutron transmission coefficients rather than try to determine equivalent spherical optical parameter sets that may be physically unrealistic or only appropriate for a limited energy range. Thus coupled-channel calculations were made using the ECIS⁴ code in which the $1/2^+$, $3/2^+$, $5/2^+$, $7/2^+$, and $9/2^+$ members of the ground state rotational band were coupled together. Actually little pertinent data exist for thulium other than s-wave strength and potential scattering radius values at low energies and total cross sections between 2.5 and 15 MeV. Our initial step was to determine a deformed optical parameter set for the neighboring nucleus ^{165}Ho for which ample data exist over a wide energy range. Such parameters reproduced concurrently total cross sections between 0.05 and 20 MeV, s- and p-wave strength functions, elastic angular distributions, and 16-MeV proton scattering data to the ground and first excited state. These parameters were applied to ^{169}Tm through use of an isospin term in the real and imaginary well depths along with adjustment of β_2 and β_4 deformation parameters based on available systematics in this mass region. Table I lists these resulting parameters along with β_2 and β_4 values.

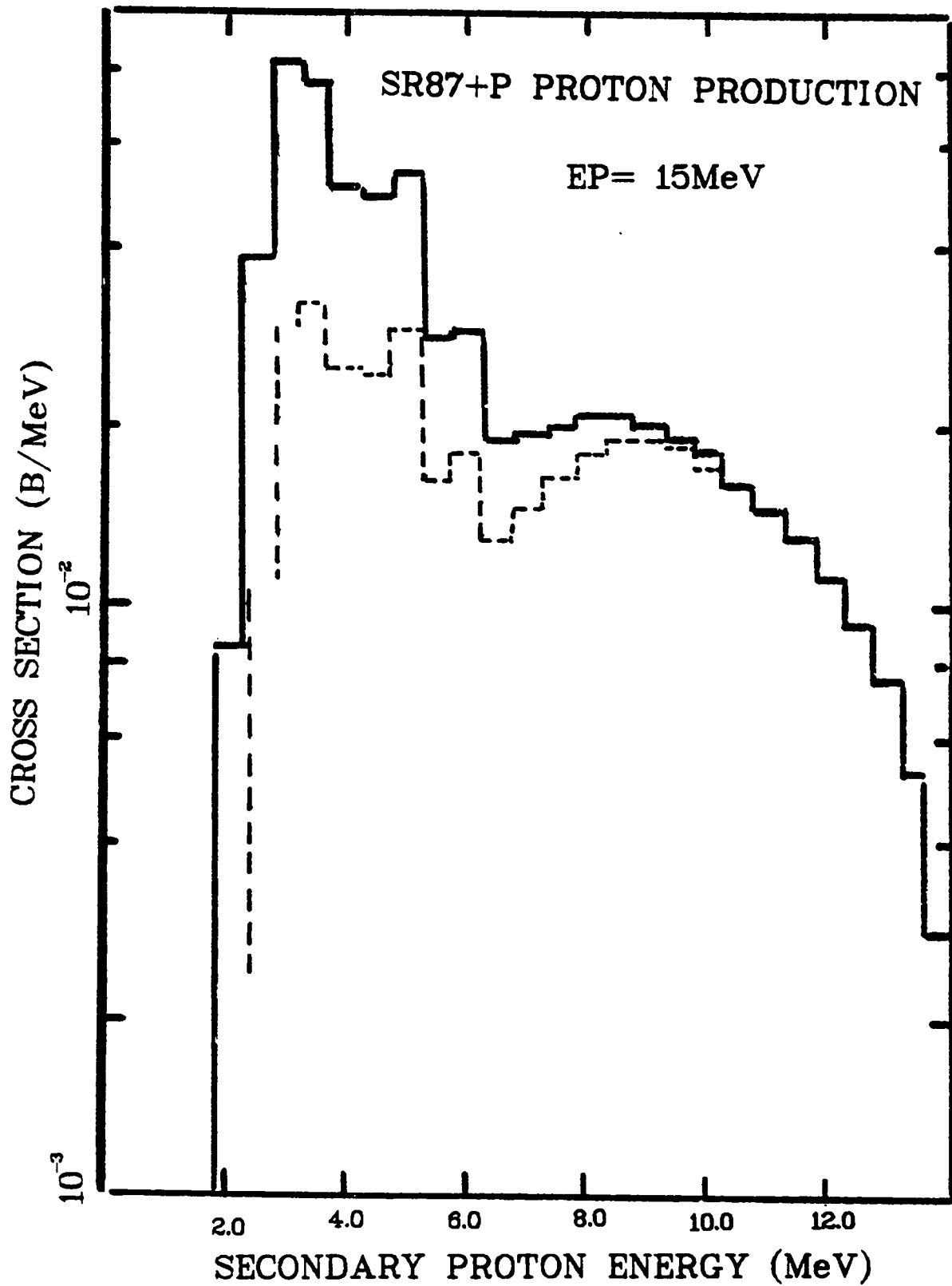


Fig. 4.

The calculated proton production spectrum induced by 15-MeV protons on ^{87}Sr showing the sensitivity of the theoretical results to the parameter changes described in Fig. 3.

TABLE I

DEFORMED OPTICAL PARAMETERS $n + {}^{169}\text{Tm}^*$

	r	a
$V = 46.87 - 0.25 E$	1.26	0.63
$W_{\text{vol}} = -1.8 + 0.2 E$	1.26	0.63
$V_{\text{SO}} = 6.$	1.26	0.63
below 6.5 MeV		
$W_{\text{SD}} = 3.6 + 0.6 E$	1.26	0.48
above 6.5 MeV		
$W_{\text{SD}} = 7.5 - 0.1 (E - 6.5)$	1.26	0.48
$\beta_2 = 0.288 \quad \beta_4 = -0.01$		

* All well depths are in MeV; geometrical parameters are in fm.

D. Statistical Model Calculations of the ${}^{169}\text{Tm}(n, \gamma) {}^{170}\text{Tm}$ Cross Section (P. G. Young and E. D. Arthur)

Within the framework of the Hauser-Feshbach statistical model, we have calculated average cross sections for the ${}^{169}\text{Tm}(n, \gamma)$ reaction between 0.001 and 3 MeV. In such statistical calculations the compound nucleus cross section for an open channel cc' having angular momentum J and parity π can be determined from⁵

$$\sigma_{cc'}^{J\pi} = \pi \lambda^2 \frac{\langle \Gamma_c \rangle^{J\pi} \langle \Gamma_{c'} \rangle^{J\pi}}{\langle \Gamma \rangle^{J\pi}} S_{cc'}^{J\pi} \quad (1)$$

where the widths $\langle \Gamma \rangle$ are determined from transmission coefficients specified by a given physical model. The width-fluctuation correction factor $S_{cc'}^{J\pi}$, accounts for the fact that these partial widths are averaged over a Porter-Thomas chi-square distribution. In our calculations such corrections were applied since they are important at lower energies. As the number of open channels increases rapidly at higher energies, the factor approaches unity above a few MeV.

The neutron transmission coefficients used in Eq. (1) were calculated from the deformed optical model parameters described in the previous section. To calculate gamma-ray transmission coefficients, we applied the Brink-Axel giant dipole resonance (GDR) model⁶ normalized to the ratio of the experimental values⁷ for the average gamma-ray width ($\langle\Gamma_\gamma\rangle = 0.084$ eV) and S-wave resonance spacing ($\langle D_0\rangle = 7.3$ eV) at the neutron binding energy. We later found it necessary to increase the $2\pi\langle\Gamma_\gamma\rangle/\langle D_0\rangle$ ratio based on these values by 10% to get good agreement with $^{169}\text{Tm}(n,\gamma)$ cross-section measurements. Two Lorentzian curves centered at energies of 12.1 and 15.5 MeV with widths 2.9 and 4.50 MeV were used to describe the shape of the GDR appropriate for a deformed nucleus. The resulting gamma-ray strength function for ^{170}Tm used in our calculations is compared in Fig. 5 to that deduced by Joly et al.⁸ from measurements of gamma-ray spectra from capture. We did not include the resonance structure at $\epsilon_\gamma = 3.5$ MeV since our calculation of the integrated cross sections should show a decreased sensitivity to such detail in the gamma-ray strength function.

A maximum amount of discrete level information was used for each residual nucleus occurring in the calculation. Such information plays a particularly important role in the description of inelastic scattering competition to the capture cross section important at higher energies. To describe the continuum of levels above the last discrete level, we employed the level density model of Gilbert and Cameron.⁹ This phenomenological model consists of a constant temperature expression appropriate for lower excitation energies and a Fermi-gas form at higher energies. Constant temperature parameters were adjusted to fit data available for the cumulative number of levels, whereas the value of the Fermi-gas parameter "a" was verified (for ^{170}Tm) through calculation of the s-wave resonance spacing at the neutron binding energy.

The calculated $^{169}\text{Tm}(n,\gamma)$ cross section is compared to experimental results in Fig. 6 up to 1 MeV. At lower energies there is good agreement between the calculation and experiment, indicating a proper choice for the gamma-ray strength function normalization. Efforts are now under way to extend the calculations to higher energies in order to compare to data available up to 3 MeV.

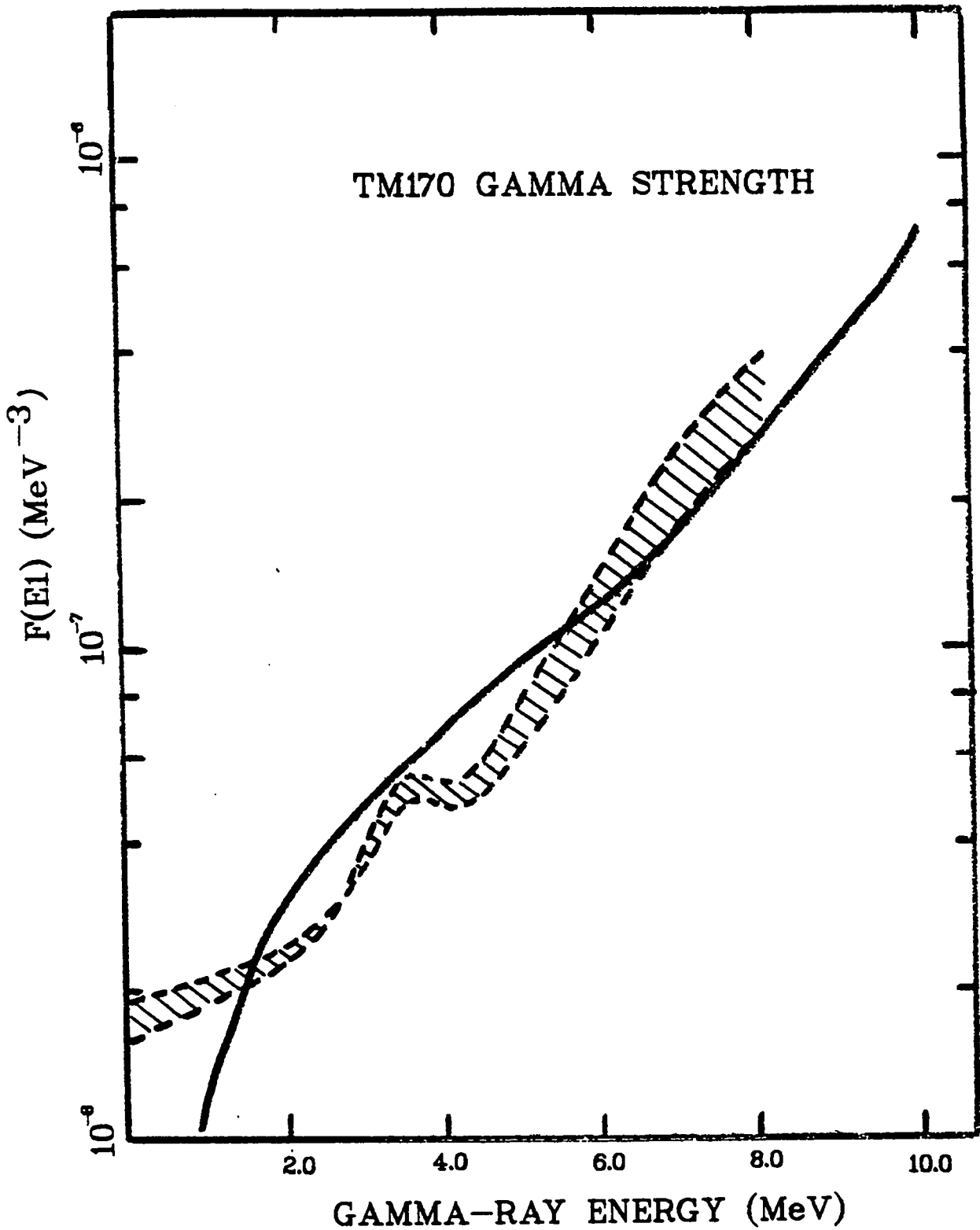


Fig. 5.

The ^{170}Tm gamma-ray strength function (solid curve) used in the present calculation is compared to that extracted from spectral $^{169}\text{Tm}(n,\gamma)$ measurements by Joly et al.⁸

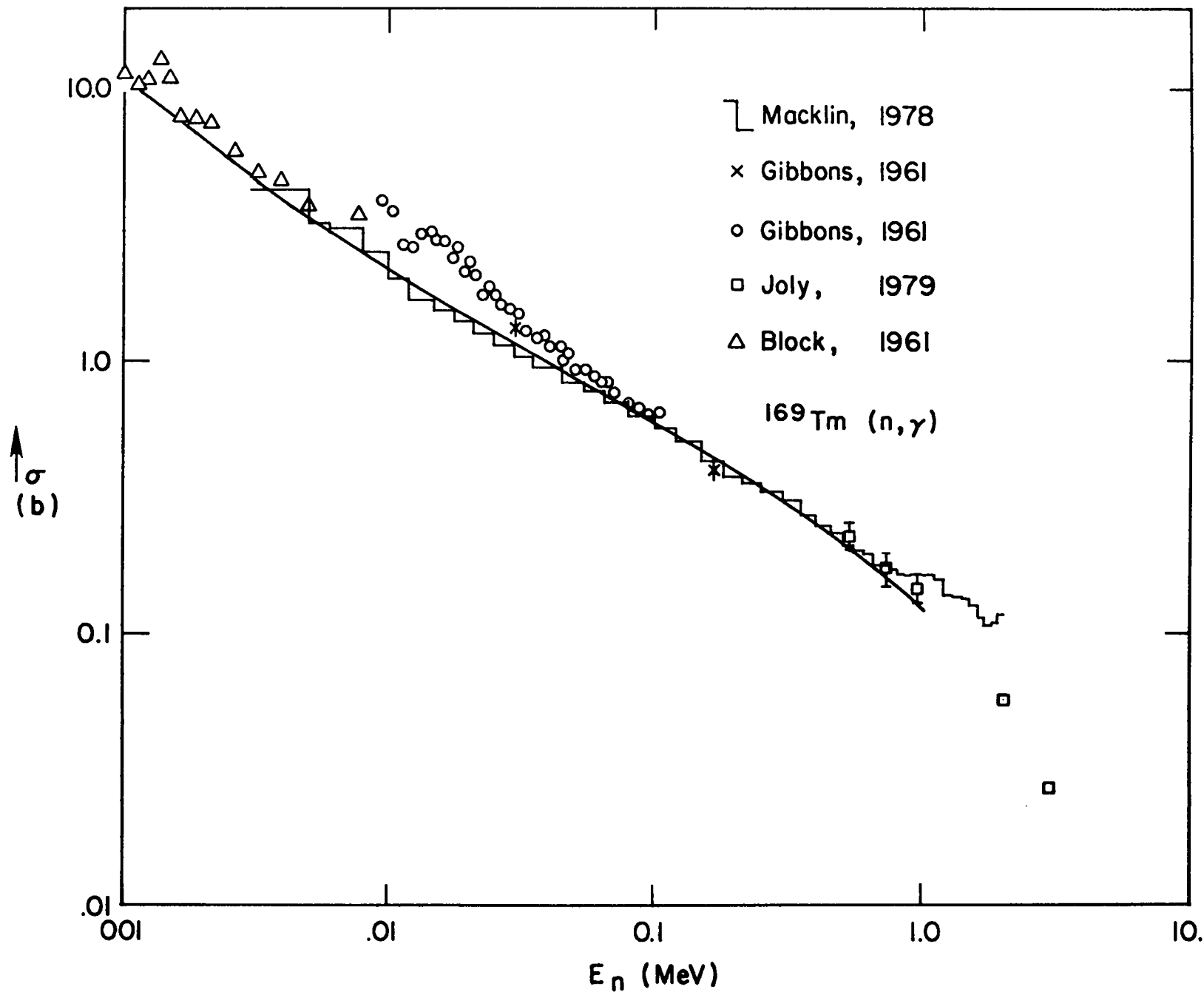


Fig. 6. Comparison of the calculated $^{169}\text{Tm}(n, \gamma)$ cross section with experimental data.

E. Statistical Model Calculations of Neutron Reactions on ^{239}Pu between 0.01 and 5 MeV (E. D. Arthur)

We have begun Hauser-Feshbach statistical model calculations of neutron reactions on ^{239}Pu between 0.01 and 5 MeV, with particular emphasis on inelastic scattering. To perform these calculations, we used the COMNUC¹⁰ Hauser-Feshbach statistical model code that includes a simple representation of the fission process using penetrabilities calculated with a single-barrier Hill-Wheeler expression.¹¹ Width-fluctuation corrections were also applied. To provide neutron transmission coefficients for these calculations, we used values generated from the ECIS⁴ coupled-channel code employing deformed optical model parameters reported previously.¹² Transmission coefficients generated in such a manner retain consistency between compound-nucleus contributions to inelastic scattering cross sections and those from direct reactions.

To constrain the statistical model calculations in the absence of a plentiful supply of experimental data for ^{239}Pu inelastic scattering, input parameters were optimized to reproduce data available for competing channels, particularly for capture and fission. Fig. 7 compares our calculated fission cross section to a representation of the average data trends over the energy range from 0.01 to 5 MeV. The bands represent $\pm 5\%$ deviations from these trends. From this analysis we deduced a fission barrier height of 5.85 MeV and a curvature of 0.85 MeV. An enhancement of the level density at the barrier (on the order of a factor of 5-10) was observed in keeping with the interpretation of enhanced rotational states resulting from asymmetries associated with the fission saddle point. These parameters produce reasonable agreement over most of the desired energy range (an exception being below 0.05 MeV) and agree well with the Back et al.¹³ inner barrier height of 5.8 ± 0.2 MeV, and $\Delta\omega = 0.8$ MeV.

Figure 8 compares our calculated angular distribution for low-lying members of the ^{239}Pu ground-state rotational band to recent data measured at Bruyeres-le-Chatel¹⁴ at an energy of 0.7 MeV. The theoretical curves include both contributions from statistical model and coupled-channel calculations. Again the agreement is satisfactory.

In summary, our initial Hauser-Feshbach calculations show reasonable agreement with available experimental data. The validity of these calculations would be improved if the fission channel representation in COMNUC were replaced with a more realistic double-humped model. Such efforts are now under way. For ^{239}Pu this is pertinent, as the outer barrier for the ^{240}Pu compound system lies

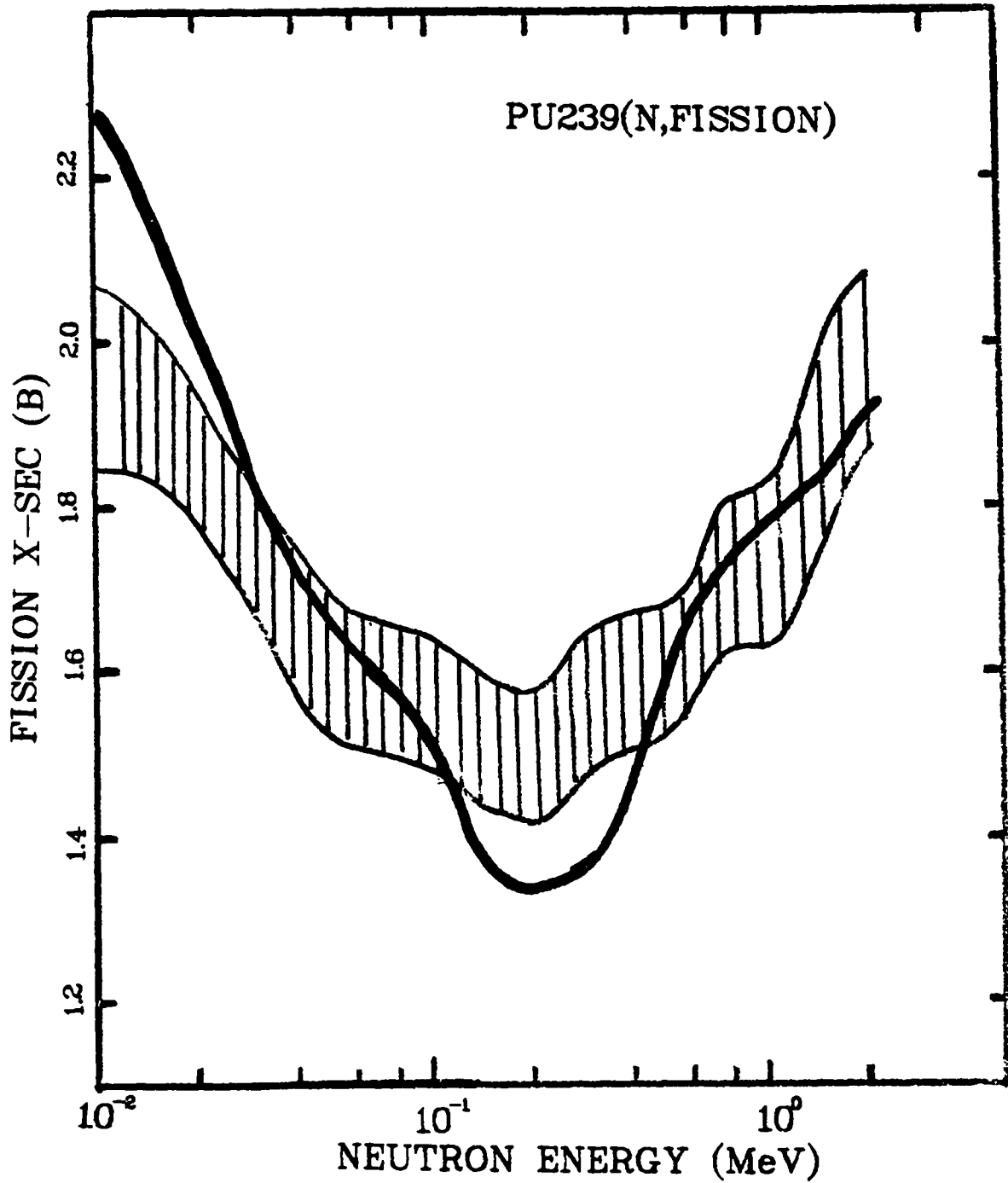


Fig. 7.

A comparison of the calculated fission cross section for ^{239}Pu (solid curve) to a representation of the average trend of the data available for the ^{239}Pu (n,f) cross section.

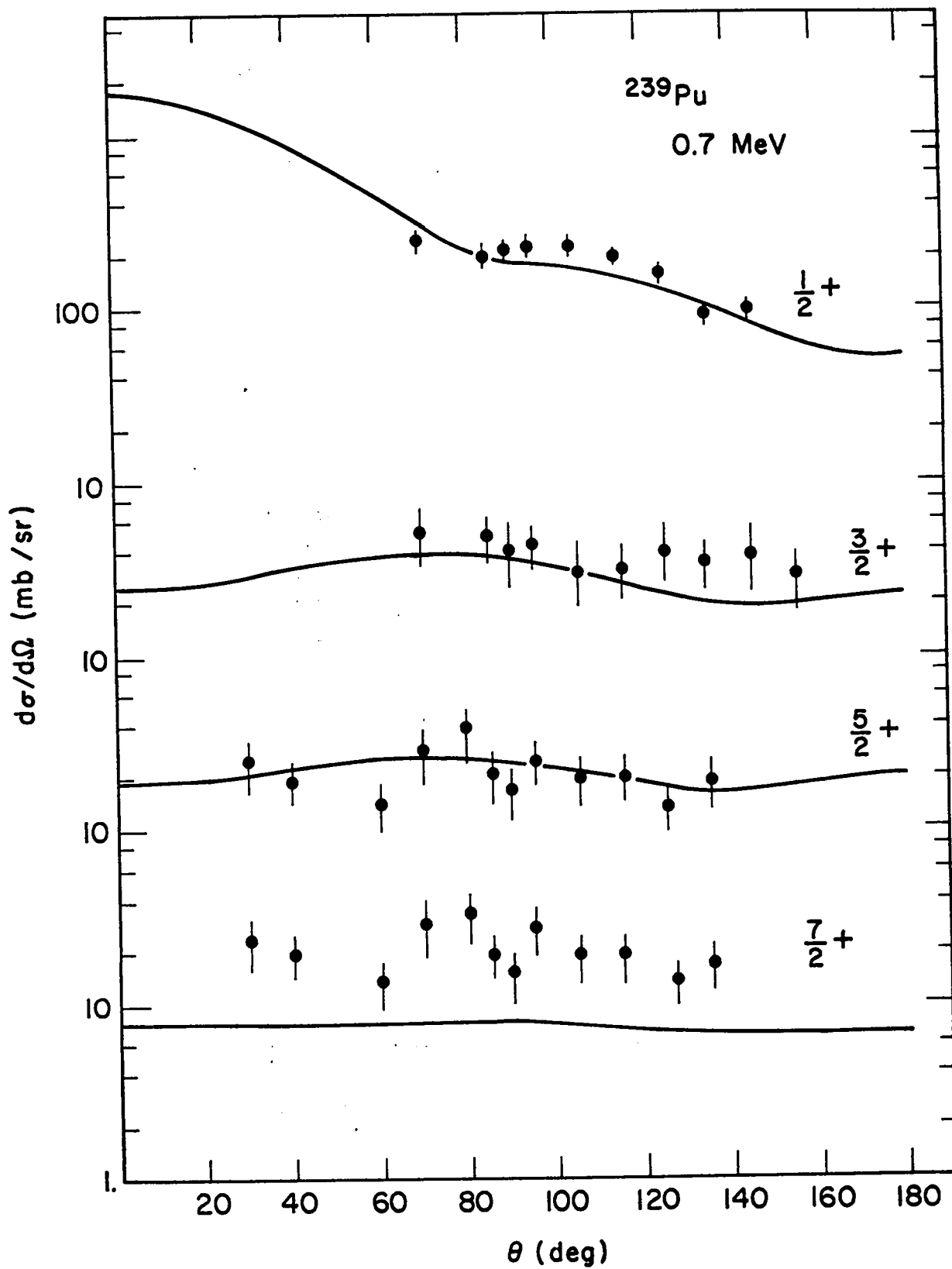


Fig. 8.

Calculated angular distributions are compared to recent measurements¹⁴ of elastic and inelastic scattering on ^{239}Pu at a neutron energy of 0.7 MeV.

approximately 350 KeV lower than the inner one,¹⁴ and a more realistic representation may result in better agreement to the fission cross section for ²³⁹Pu.

F. New Fission Neutron Spectrum Representation for Evaluated Nuclear Data Files (D. G. Madland, R. J. LaBauve, R. E. MacFarlane, and P. G. Young)

On the basis of recent theoretical work on prompt fission neutron spectra,¹⁵⁻²⁰ we propose a new fission neutron spectrum representation for use in evaluated nuclear data files. The predictive abilities of the new representation have previously been tested by detailed comparisons^{19,20} with experimental spectra, and the good agreement that has been obtained forms the basis of our proposal. We summarize here a description of the new representation, some comparisons with evaluated spectra, and the first test of its predictive ability in integral benchmark calculations. Concurrently, a more extensive proposal document is in preparation.

The new prompt fission neutron spectrum $N(E)$ is based on nuclear-evaporation theory and accounts for the effects of (1) the motion of the fission fragments, (2) the distribution of fission-fragment residual nuclear temperature, and (3) the energy dependence of the inverse process of compound-nucleus formation. We simulate the energy dependence of the inverse process by adjusting the nuclear level-density parameter to an effective value a_{eff} . This simulation permits $N(E)$ to be expressed in the closed form

$$N(E) = \frac{1}{2} (N(E, E_f^L) + N(E, E_f^H)) \quad , \quad (2)$$

where

$$N(E, E_f) = \frac{1}{3\sqrt{E_f T_m}} \left[u_2^{3/2} E_1(u_2) - u_1^{3/2} E_1(u_1) + \gamma(3/2, u_2) - \gamma(3/2, u_1) \right] \quad (3)$$

with E the laboratory energy of the emitted neutron, E_f the kinetic energy per nucleon in either the light (L) or heavy (H) fragment, T_m the maximum temperature of the fragment temperature distribution, $E_1(x)$ the exponential integral,²¹ $\gamma(a, x)$ the incomplete gamma function,²¹ $u_1 = (\sqrt{E} - \sqrt{E_f})^2/T_m$, and $u_2 = (\sqrt{E} + \sqrt{E_f})^2/T_m$. The exponential integral and incomplete gamma functions are available as program library functions on any modern scientific computer.

The evaluation of $N(E)$ requires three input parameters E_f^L , E_f^H , and T_m . The first two parameters are obtained using the experimental results of Unik et al.²² whereas T_m is given by

$$T_m = \left((\langle E_r \rangle + B_n + E_n - \langle E_f^{\text{tot}} \rangle) / a_{\text{eff}} \right)^{1/2}, \quad (4)$$

where $\langle E_r \rangle$ is the average energy release,^{23,24} B_n and E_n are the separation energy and kinetic energy of the neutron inducing fission, $\langle E_f^{\text{tot}} \rangle$ is the total average fission-fragment kinetic energy,²¹ and $a_{\text{eff}} = A/(10 \text{ MeV})$ with A the mass number of the fissioning nucleus. This is the current value of a_{eff} based on our studies to date. E_f^L , E_f^H , and T_m can be calculated for an arbitrary fissioning nucleus at a given excitation energy using Refs. 14, 16, and 17.

In Figs. 9 and 10 we compare the shape of the new spectrum (LA-Theory) to the shapes of Maxwellian (LA-Maxwell) and Watt (LA-Watt) spectra calculated for the same system and constrained by theoretical considerations^{15,17,19} to the same value of the average energy $\langle E \rangle = 2.060 \text{ MeV}$. We also compare the new spectrum to the evaluated National Bureau of Standards five-segment spectrum²⁵ with $\langle E \rangle = 1.977 \text{ MeV}$ and the evaluated ENDF/B-V Watt spectrum²⁶ with $\langle E \rangle = 2.031 \text{ MeV}$. The shape differences among the five spectra are more clear in Fig. 10 with the most significant differences involving the three spectra, which reproduce various experiments (the new theoretical spectrum and the two evaluated spectra).

A measure of the importance of the shape differences for these three spectra has been obtained by calculating one thermal and one fast integral benchmark. The calculations were performed using ENDF/B-V cross sections and the results are given in Table II. These demonstrate (a) that the shape differences between the spectra are significant relative to the standard deviations of the integral experiments and (b) the fact that there was no adjustment in the Los Alamos theory emphasizes its predictive capability.

In future work we expect to study the effects of the new fission spectrum on a variety of uranium and plutonium systems of varying spectral hardness. This work will further test the generality of the theory. For evaluation purposes we expect to fit individual cases by slight adjustments in the level-density parameter a_{eff} . This approach, however, will require extensive comparisons with high quality experimental measurements for each individual case.

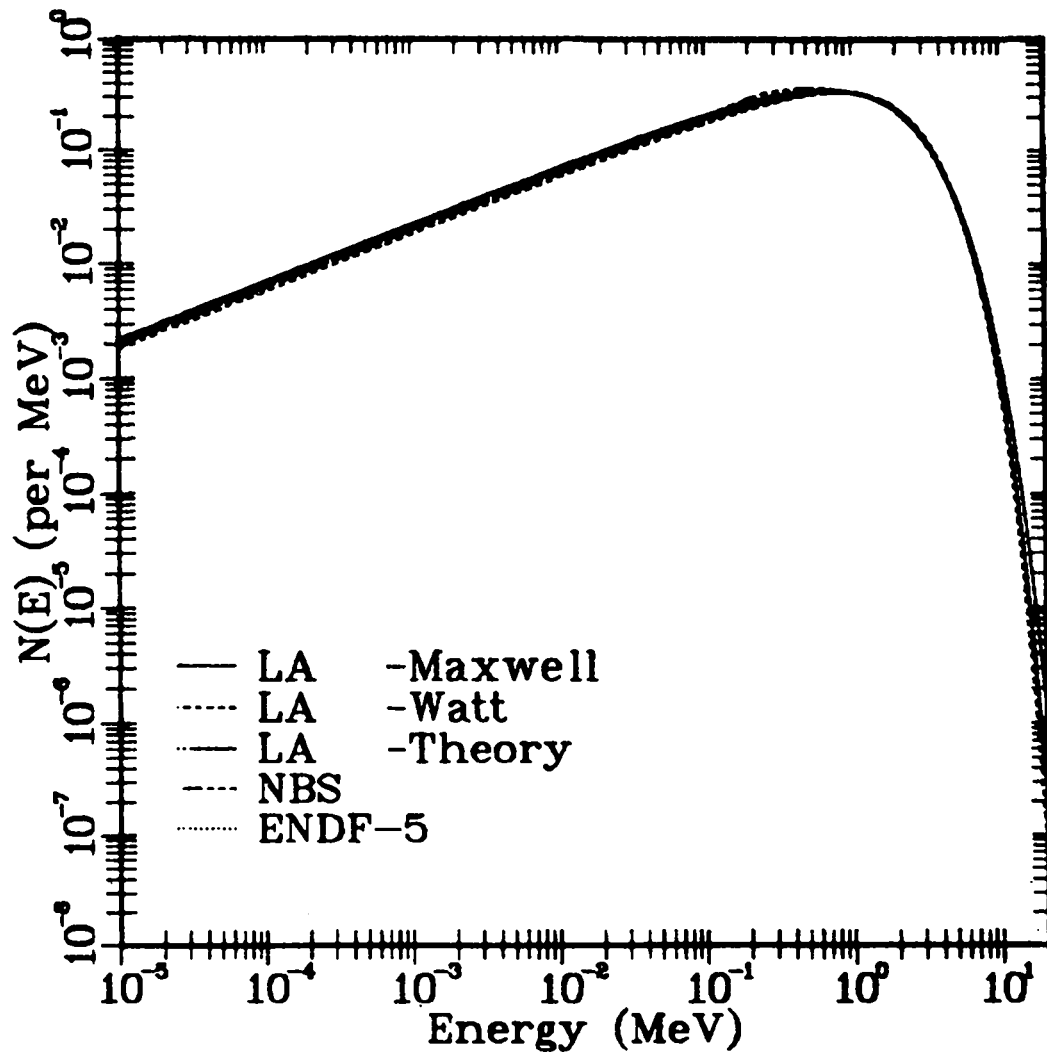


Fig. 9.

Prompt fission neutron spectra for the thermal-neutron-induced fission of ^{235}U . The new Los Alamos National Laboratory spectrum (LA-Theory), the NBS spectrum, and the ENDF/B-V spectrum all reproduce certain experimental data sets and are the basis of comparison in the integral benchmark calculations discussed in the text.

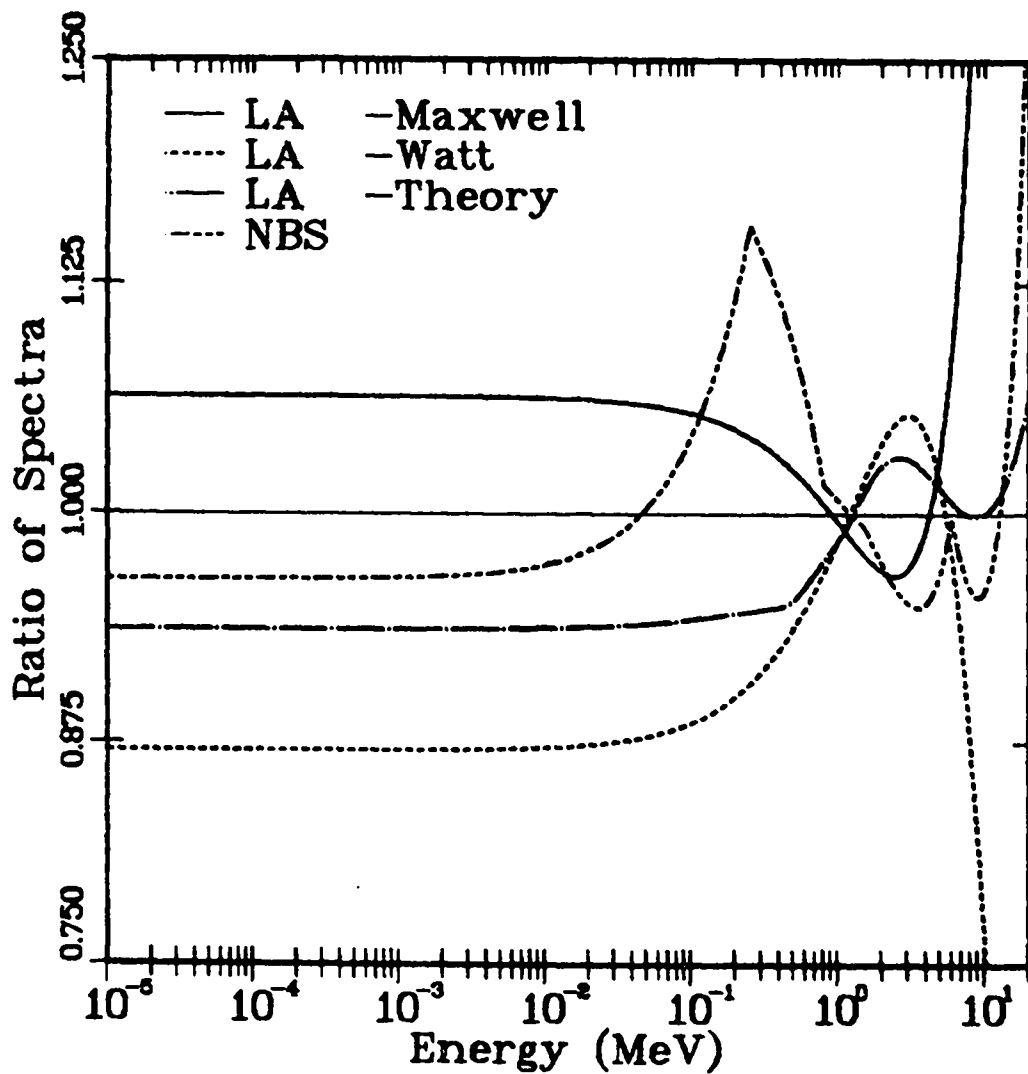


Fig. 10.

Prompt fission neutron spectra for the thermal-neutron-induced fission of ^{235}U plotted as ratios to the ENDF/B-V Watt spectrum. The new Los Alamos National Laboratory spectrum (LA-Theory), the NBS spectrum, and the ENDF/B-V spectrum all reproduce certain experimental data sets and are the basis of comparison in the integral benchmark calculations discussed in the text.

TABLE II
EFFECTS OF DIFFERENT FISSION SPECTRUM (χ) MODELS FOR TWO INTEGRAL BENCHMARKS^a

<u>Test</u>	<u>χ</u>	<u>k</u>	<u>Fission Ratio^b</u>
ORNL-1 ^c	ENDF/B-V	0.99995	2.833×10^{-4}
ORNL-1	NBS	1.00292	2.728×10^{-4}
ORNL-1	LA-Theory	0.99736	2.917×10^{-4}
ORNL-1	Experiment	1.00026	
<hr/>			
GODIVA ^d	ENDF/B-V	1.00015	0.1694
GODIVA	LA-Theory	1.00183	0.1762
GODIVA	Experiment	1.0 ± 0.001	0.1647

^a ORNL-1 is a uranyl-nitrate solution sphere dominated by thermal fission, and GODIVA is an enriched uranium metal sphere dominated by fast fission (see Ref. 27).

^b $^{238}\text{U}(n,f)/^{235}\text{U}(n,f)$ at center of assembly.

^c 69 groups, P3/S8, 40 intervals, for all ORNL-1 calculations.

^d 30 groups, P4/S16, 40 intervals, for all GODIVA calculations.

G. Calculation of Excited State Cross Sections for Actinide Nuclei (David G. Madland)

Work is continuing on the development of the excited-state coupled-channel code JUPXST.²⁸ Four states of a rotational band can now be coupled for the excited state problem. In addition, the integrated cross sections for all coupled states are calculated, and the multipole expansion of the deformed potential has been extended from $\lambda = 4$ up through $\lambda = 8$ for both the real and imaginary central terms. The next step is to perform an actual calculation over an energy range of about 10 keV to 10 MeV for a target nucleus in both the ground state and in the first excited state.

II. NUCLEAR CROSS-SECTION PROCESSING AND TESTING

A. Los Alamos National Laboratory - Benchmark Calculations (R. B. Kidman)

The new and revised benchmark specifications²⁹ for nine Los Alamos National Laboratory critical assemblies are being employed to compute the entire set of parameters that were measured in the experiments. A comparison between the computed and experimental values should provide a measure of the adequacy of the specifications, cross sections, and physics codes used in the calculations.

Part of the effort has been to determine eigenvalue behavior as a function of Legendre scattering order and as a function of angular quadrature. The results, shown in Tables III and IV, were computed with transport theory³⁰ using infinitely dilute cross sections and 70-group vector fission sources. The cross sections and fission source data were generated with NJOY³¹ from ENDF/B-V³² data. $P_{1/2}$ refers to the results of using transport corrected P_0 cross sections. Accurate P_∞ and S_∞ eigenvalue estimates can be produced from these tables.

If one assumes that improvements like self-shielding or fission source matrices will not change the eigenvalue behavior significantly, then the results in Tables III and IV can be used to convert more refined calculations to $P_\infty S_\infty$ results.

B. Processed Multigroup and Few-Group Cross Sections [(W. B. Wilson, T. R. England, R. J. LaBauve, R. M. Boicourt, N. L. Whittemore, and R. E. Schenter (Hanford Eng. Development Lab.))]

For use in a wide variety of applications, all ENDF/B-V fission product and actinide cross sections have been processed into 154 groups using the NJOY code³¹ at three temperatures, and additionally, three or more Bondarenko background cross sections have been used to simulate self-shielding in the actinides. The multigroup structure and a collapsing code are described in a document completed during this quarter and sent to the Electric Power Research Institute (EPRI) for final publication and distribution.³³ The multigroup library contains $\approx 223\ 059$ card records; this library and a collapsing code are described in the document.

TABLE III

EIGENVALUE vs LEGENDRE ORDER (ALL S_{16})

	<u>P₀</u>	<u>P_{1/2}</u>	<u>P₁</u>	<u>P₂</u>	<u>P₃</u>	<u>P₄</u>	<u>P₅</u>
Jezebel	1.099107	1.012750	1.003351	1.009515	1.009407	1.009411	1.009410
Jezebel-23	1.104118	0.998695	0.987885	0.994773	0.994688	0.994692	0.994691
Jezebel-Pu	1.092024	1.004189	0.994834	1.000952	1.000852	1.000856	1.000855
Bigten	1.065059	1.012091	1.010722	1.011627	1.011591	1.011595	1.011594
Godiva	1.111715	1.004524	0.995863	1.001335	1.001287	1.001293	1.001291
Flattop-23	1.148283	1.016788	0.985888	1.013658	1.005577	1.007753	1.007196
Thor	1.151387	1.028662	0.991730	1.026523	1.015258	1.018901	1.017836
Flattop-Pu	1.159393	1.023888	0.990812	1.019677	1.011958	1.013995	1.013496
Flattop-25	1.146298	1.017309	0.994933	1.012890	1.009223	1.010013	1.009849

TABLE IV

EIGENVALUE vs ANGULAR QUADRATURE (all P_3)

	<u>S₄</u>	<u>S₈</u>	<u>S₁₆</u>	<u>S₃₂</u>	<u>S₄₈</u>
Jezebel	1.021764	1.012103	1.009407	1.008665	1.008522
Jezebel-23	1.005988	0.997147	0.994688	0.994009	0.993878
Jezebel-Pu	1.012844	1.003465	1.000852	1.000131	0.999992
Bigten	1.012258	1.011723	1.011591	1.011555	1.011548
Godiva	1.009787	1.003115	1.001287	1.000778	1.000679
Flattop-23	1.022704	1.008602	1.005577	1.004737	1.004561
Thor	1.035998	1.019100	1.015258	1.014254	1.014048
Flattop-Pu	1.030267	1.015254	1.011958	1.011072	1.010900
Flattop-25	1.021648	1.011491	1.009223	1.008612	1.008494

For inclusion in a general reference document³⁴ listing major decay, yield, and absorption parameters, the cross sections were collapsed to one group in six fast reactor spectra and into four groups using a typical LWR thermal reactor spectra. The four-group structure is described in Table V and the LWR spectrum is listed in Ref. 34. The fast weighting functions used in collapsing the cross sections cover a wide range of fast spectra typically in use for various reactors in the core and, in one case, the softer spectra in the reflector region. The 1 KMW core values are used in general survey calculations. The four-group thermal values can be used for almost all commercial LWRs provided that the effective thermal cross section is multiplied by $\langle\sigma_{1/v}\rangle$, which is the average of a $1/v$ dependent cross section that is unity at 0.0253 eV. (In the spectra used in processing and collapsing, this average is 0.554018.) This procedure effectively accounts for variations in the thermal spectra of various reactors.

The one and four group values are all based on a collapsing of the infinitely dilute multigroup values processed at 900°F. That is, all values are Doppler broadened for this temperature, but there is no self-shielding. Few-group values for all 237 nuclides, cross sections, and resonance integrals will be tabulated in a forthcoming report.

TABLE V

FOUR GROUP ENERGY STRUCTURE

<u>Group</u>	<u>Energy (eV)</u>
	10^7
1	8.20850×10^5
2	5.53085×10^3
3	6.2506×10^{-1}
4	10^{-5}

C. Integral Cross Sections in Three Representations of the ^{252}Cf Spontaneous Fission Spectrum (R. J. LaBauve, D. G. Madland, R. E. MacFarlane, P. G. Young, and R. M. Boicourt)

Three representations of the ^{252}Cf spontaneous fission spectrum were used as weighting functions in calculating several integral cross sections for which good measurements are available. The ^{252}Cf s.f. spectrum representations used include the NBS ^{252}Cf spectrum³⁵ and two Los Alamos theoretical models, namely, an "exact theory" and an approximate model that is more suitable for inclusion in ENDF (see sec. I.F. p. 15). It should be emphasized that the parameters used in the Los Alamos models so far have not been adjusted to fit experimental ^{252}Cf s.f. spectrum measurements.

The NBS representation of the ^{252}Cf s.f. spectrum $\chi(E)$ consists of five segments given by a reference Maxwellian $M_{\text{Cf}}(E)$ times a correction term $\mu(E)$ defined for each of five energy ranges as follows.

$$\chi(E) = \mu(E) M_{\text{Cf}}(E), \text{ where}$$

$$M_{\text{Cf}}(E) = 0.6672 \sqrt{E} \exp(-1.5E/2.13), \text{ E in MeV}$$

and

from 0.0 to 0.25 MeV	$\mu(E) = 1 + 1.20E - 0.237$
from 0.25 to 0.8 MeV	$\mu(E) = 1 - 0.14E + 0.098$
from 0.8 to 1.5 MeV	$\mu(E) = 1 + 0.024E - 0.0332$
from 1.5 to 6.0 MeV	$\mu(E) = 1 - 0.0006E + 0.0037$
above 6.0 MeV	$\mu(E) = 1.0 \exp[-0.03(E - 6.0)]/1.0$

In Fig. 11 the two Los Alamos ^{252}Cf s.f. spectrum representations are compared as ratios to the NBS representation.

In Ref. 36 several accurate measurements of spectral indexes in the ^{252}Cf s.f. spectrum are discussed; that is, the ratios of the integral cross sections in the ^{252}Cf spectrum for several reactions are given as ratios to the integral $^{238}\text{U}(n,f)$ cross section. These spectral indexes can be transformed into integral cross sections by using a value for the integral $^{238}\text{U}(n,f)$ cross section in the ^{252}Cf s.f. spectrum as measured by Gilliam.³⁷ The integral cross-section values so derived can then be directly compared with calculations using the two Los Alamos models and the NBS representation of the ^{252}Cf s.f. fission spectrum. Results comparing experimental to calculated values are given in Table VI.

TABLE VI

INTEGRAL CROSS SECTIONS (mb) IN THREE ^{252}Cf S.F. SPECTRA

Threshold Reactions	Observed $\pm (1\sigma)$	NBS		LA Exact Theory		LA Approx. Theory	
		Calculated	C/E	Calculated	C/E	Calculated	C/E
$^{115}\text{In}(n,n')$	195. $\pm 5.$	182.	0.933	190.	0.974	193.	0.990
$^{47}\text{Tl}(n,p)$	19.6 ± 0.5	24.1	1.230	25.7	1.311	26.2	1.337
$^{58}\text{Ni}(n,p)$	118. $\pm 3.$	114.	0.996	122.	1.034	125.	1.059
$^{54}\text{Fe}(n,p)$	87.4 ± 2.1	88.3	1.010	94.6	1.082	96.8	1.108
$^{46}\text{Tl}(n,p)$	14.2 ± 0.4	13.5	0.951	14.7	1.035	14.9	1.049
$^{56}\text{Fe}(n,p)$	1.45 ± 0.04	1.41	0.972	1.59	1.097	1.58	1.090
$^{48}\text{Tl}(n,p)$	0.424 ± 0.011	0.409	0.965	0.465	1.097	0.456	1.075
$^{27}\text{Al}(n,\alpha)$	1.027 ± 0.023	1.059	1.031	1.207	1.175	1.183	1.152
<u>Non-Threshold Reactions</u>							
$^{238}\text{U}(n,f)$	319. $\pm 8.$	313.	0.981	329.	1.031	334.	1.047
$^{197}\text{Au}(n,\gamma)$	81. ± 1.9	76.7	0.947	72.9	0.900	72.3	0.893
$^{235}\text{U}(n,f)$	1205. $\pm 27.$	1236.	1.026	1237.	1.027	1237.	1.027
$^{239}\text{Pu}(n,f)$	1802. $\pm 40.$	1792.	0.994	1799.	0.998	1800.	0.999
$^{237}\text{Np}(n,f)$	1332. $\pm 37.$	1352.	1.015	1385.	1.040	1390.	1.044
	Average	C/E	1.004		1.061		1.067

All cross sections used in the calculations were taken from ENDF/B-V dosimetry files³⁸ and processing was done with the NJOY code.³¹ The results were verified by R. Seamon and R. Little of Los Alamos using the MARK code.³⁹ Figures 11-24 show the ENDF/B-V microscopic cross sections compared with the three spectra.

The agreement between calculation and experiment seen in Table VI is quite good, especially for the NBS representation. The agreement for the Los Alamos spectra could undoubtedly be improved by adjusting the theoretically derived parameters used in the models.

Of course, these calculations are also a check of the validity of the ENDF/B-V dosimetry data; the $^{47}\text{Ti}(n,p)$ and $^{197}\text{Au}(n,\gamma)$ cross sections are the most discrepant. It should be noted, however, that in another analysis of measured integral neutron cross sections in the ^{252}Cf s.f. spectrum,⁴⁰ a value of 76.2 ± 1.8 mb is given for the $^{197}\text{Au}(n,\gamma)$ integral cross section. Other values given in this analysis agree more closely with those derived from Ref. 35.

One additional recent measurement was also used in comparing the three representations of the ^{252}Cf s.f. spectrum. This is the $^{63}\text{Cu}(n,\alpha)$ integral cross section measured by Winkler et al.⁴¹ These observers obtained a value of 0.709 ± 0.017 mb, which is to be compared with calculations using ENDF/B-V microscopic cross sections of 0.758 for the NBS spectrum, 0.850 for the "exact" and 0.844 with the "approximate" Los Alamos ^{252}Cf s.f. spectrum models. Comparison of the $^{63}\text{Cu}(n,\alpha)$ cross section with the three spectra is shown in Fig. 25. All measurements will be useful in future checking of adjusted parameters for the Los Alamos models.

D. NJOY Development (R. E. MacFarlane, D. W. Muir, R. M. Boicourt)

A new version of NJOY is in the final stages of preparation, and it includes a number of new features. The formatted output routine has been modified to output numbers in the form $n.nnnnnn\pm e$ when only one digit is required for the exponent field. This allows increased precision in resonance reconstruction for materials like ^{238}U . The RECONR module now has NDIGIT as an input parameter for user convenience. Values of 6 or 7 are normal, but even more digits can be used if formatted output is not required. The resonance reconstruction algorithm in RECONR has also been modified to include a resonance integral check in addition to the normal check for linearity within a specified tolerance. In addition, some of the loops were reorganized to be vectorizable by the Cray FORTRAN compiler (CFT).

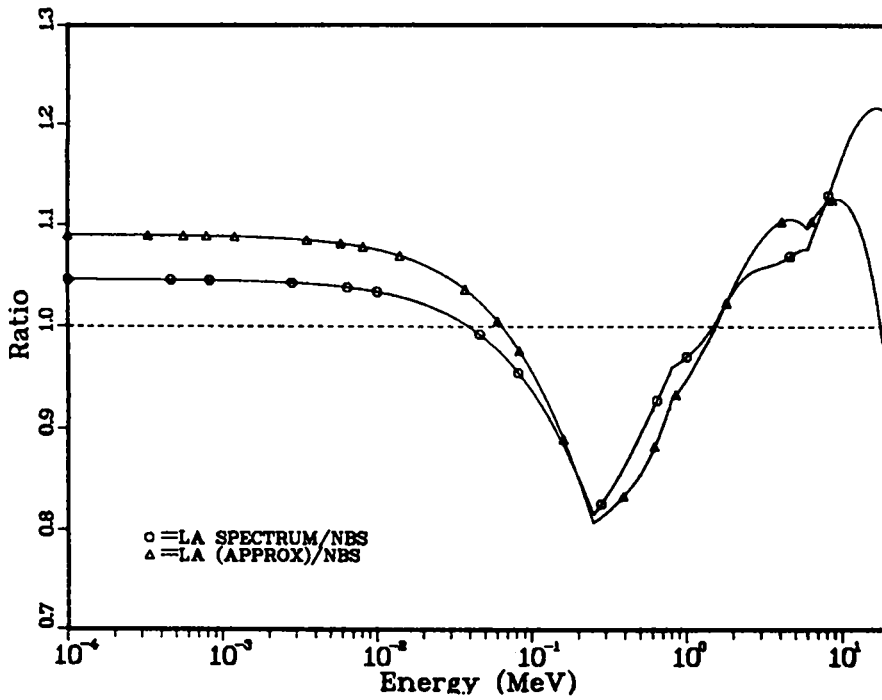


Fig. 11.
 Comparison of two Los Alamos representations
 of the ^{252}Cf s.f. spectrum as ratios to the
 National Bureau of Standards representation.

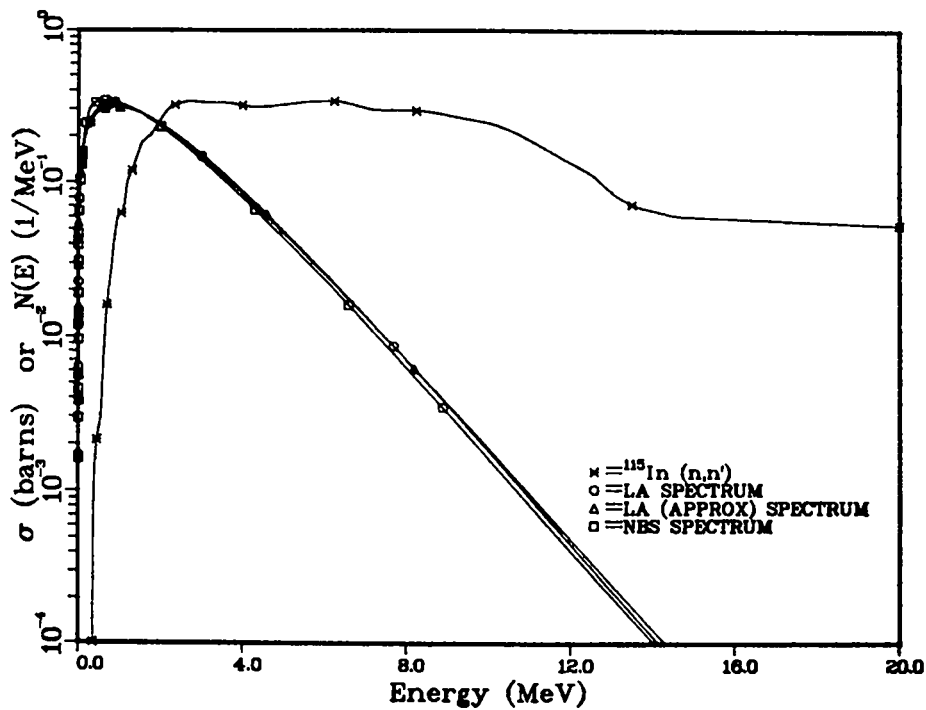


Fig. 12.
 The $^{115}\text{In}(n,n')$ cross section compared with three
 representations of the ^{252}Cf s.f. spectrum.

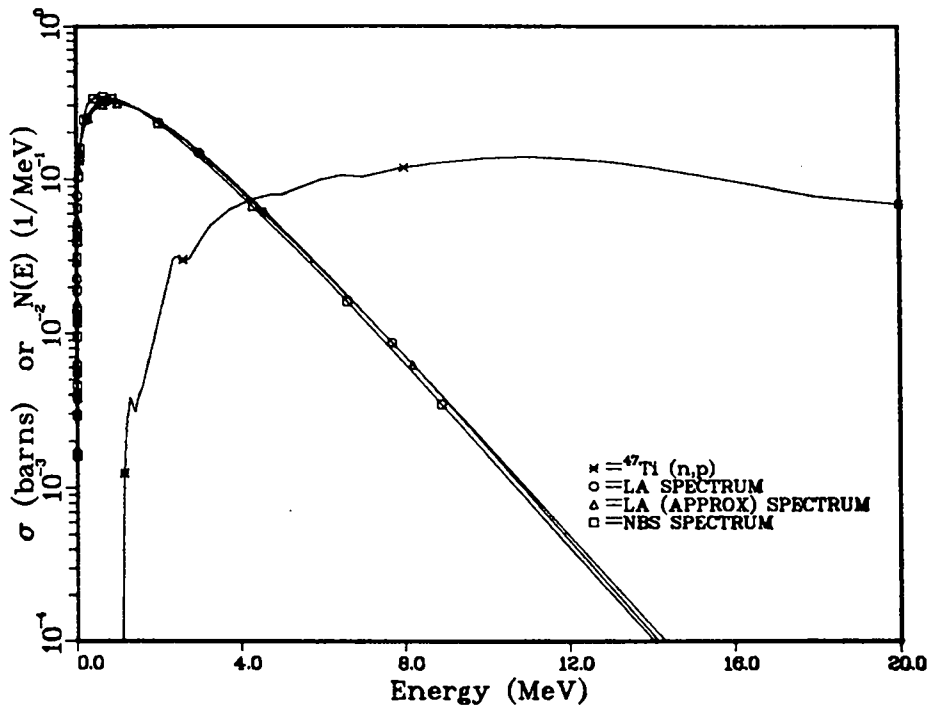


Fig. 13.
The $^{47}\text{Ti}(n,p)$ cross section compared with three representations of the ^{252}Cf s.f. spectrum.

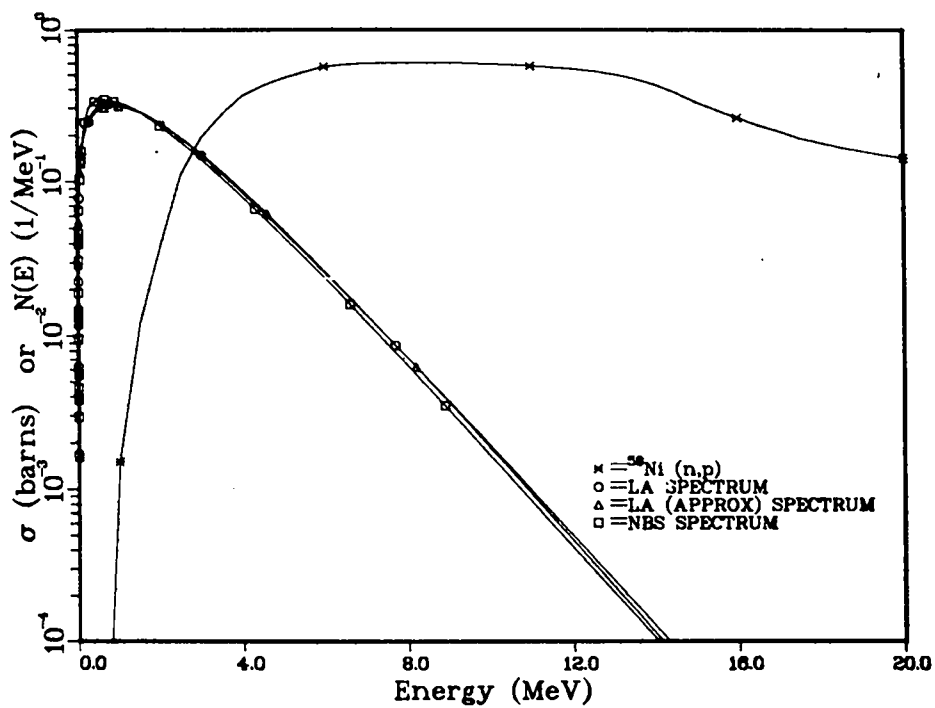


Fig. 14.
The $^{58}\text{Ni}(n,p)$ cross section compared with three representations of the ^{252}Cf s.f. spectrum.

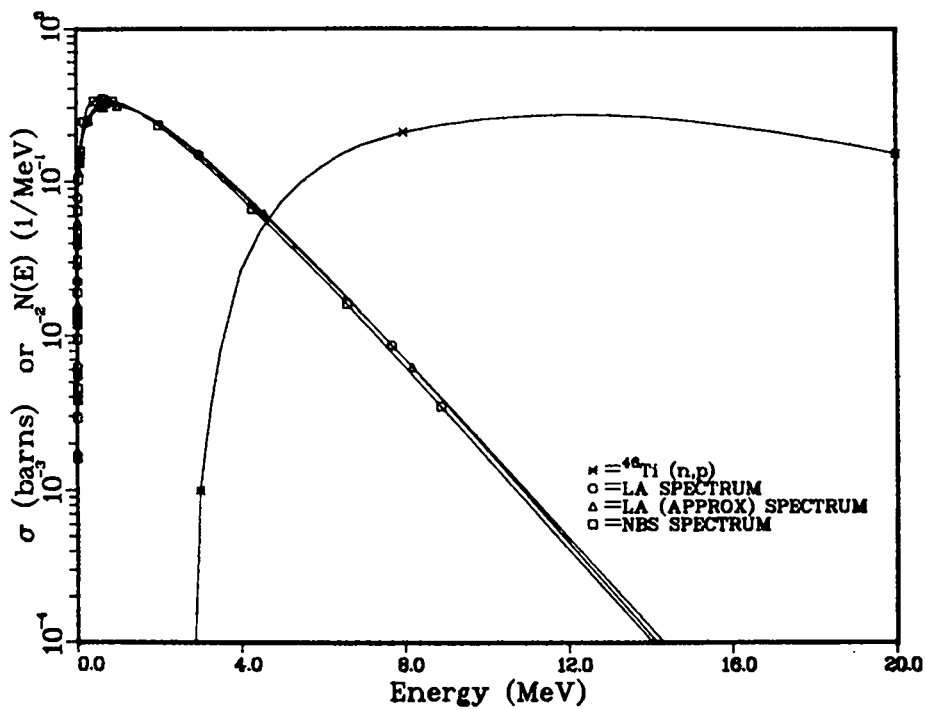


Fig. 15.
 The $^{46}\text{Ti}(n,p)$ cross section compared with three representations of the ^{252}Cf s.f. spectrum.

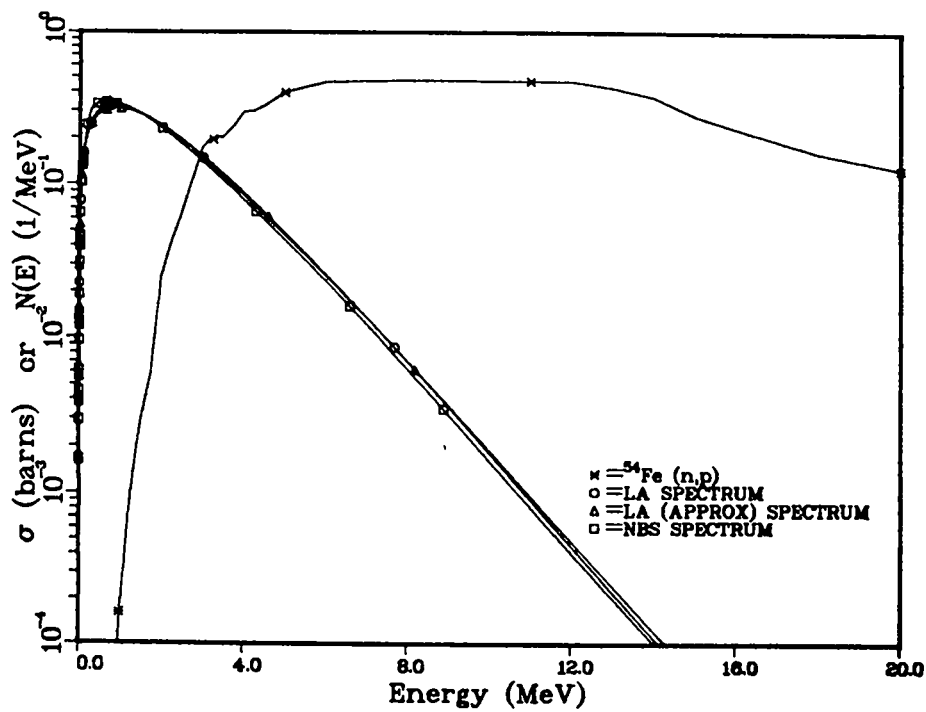


Fig. 16.
 The $^{54}\text{Fe}(n,p)$ cross sections compared with three representations of the ^{252}Cf s.f. spectrum.

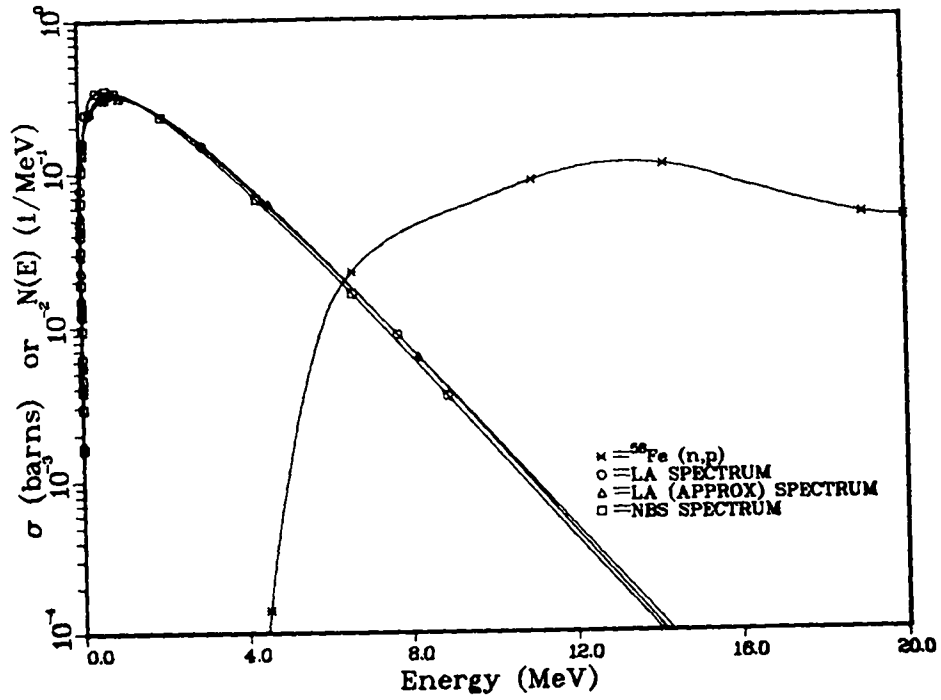


Fig. 17.
The $^{56}\text{Fe}(n,p)$ cross section compared with three representations of the ^{252}Cf s.f. spectrum.

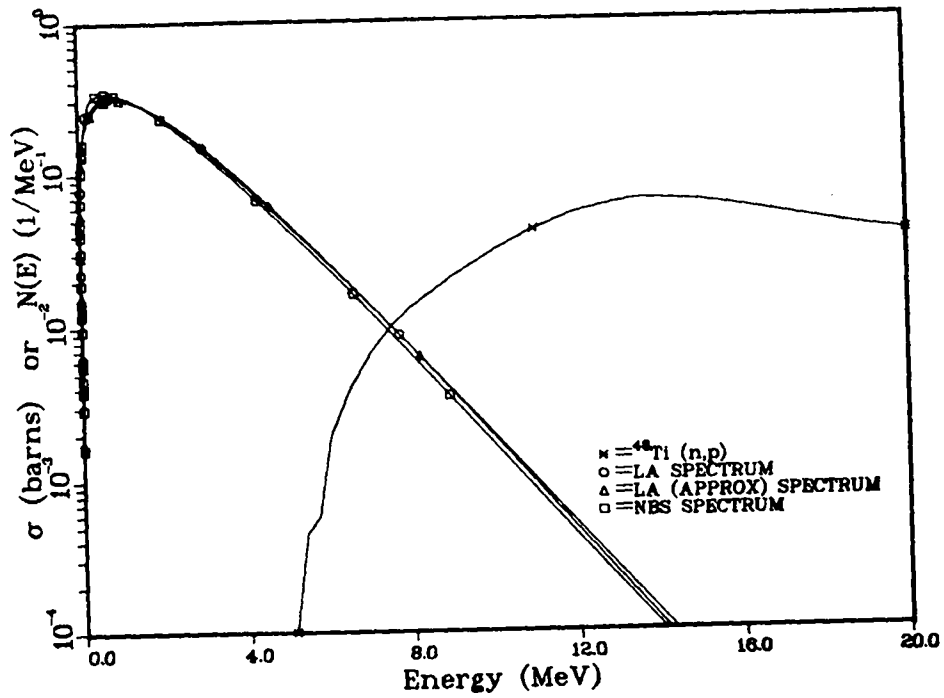


Fig. 18.
The $^{48}\text{Ti}(n,p)$ cross section compared with three representations of the ^{252}Cf s.f. spectrum.

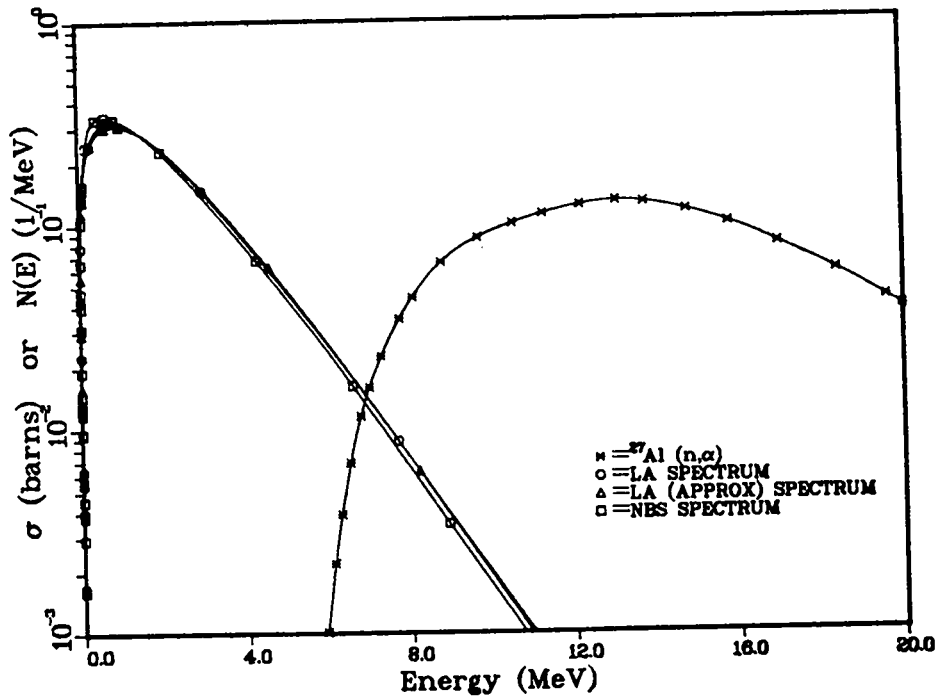


Fig. 19.
The $^{27}\text{Al}(n,\alpha)$ cross section compared with three representations of the ^{252}Cf s.f. spectrum.

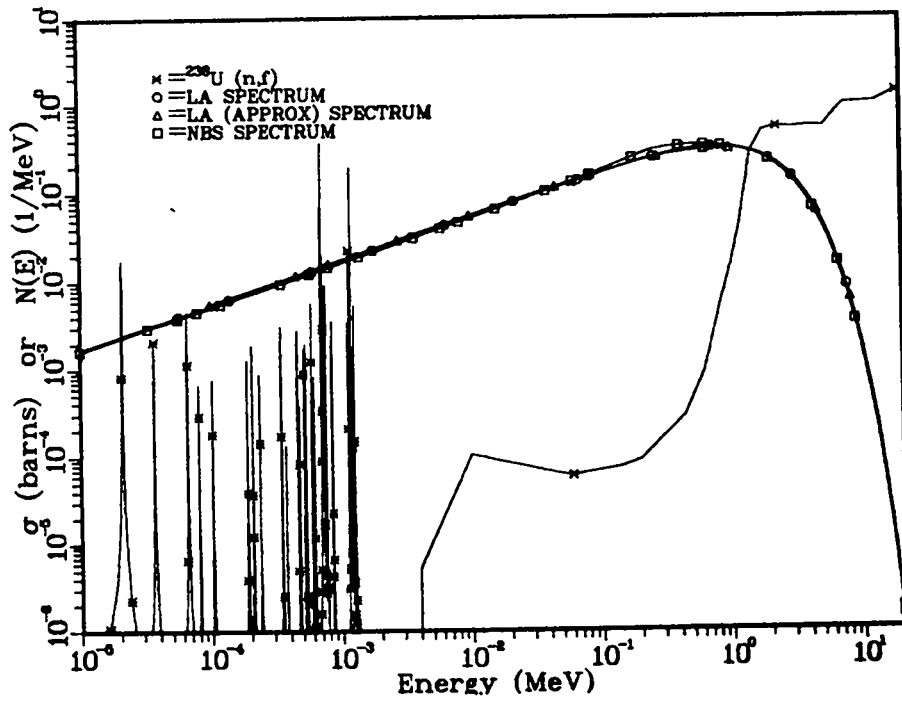


Fig. 20.
The $^{238}\text{U}(n,f)$ cross section compared with three representations of the ^{252}Cf s.f. spectrum.

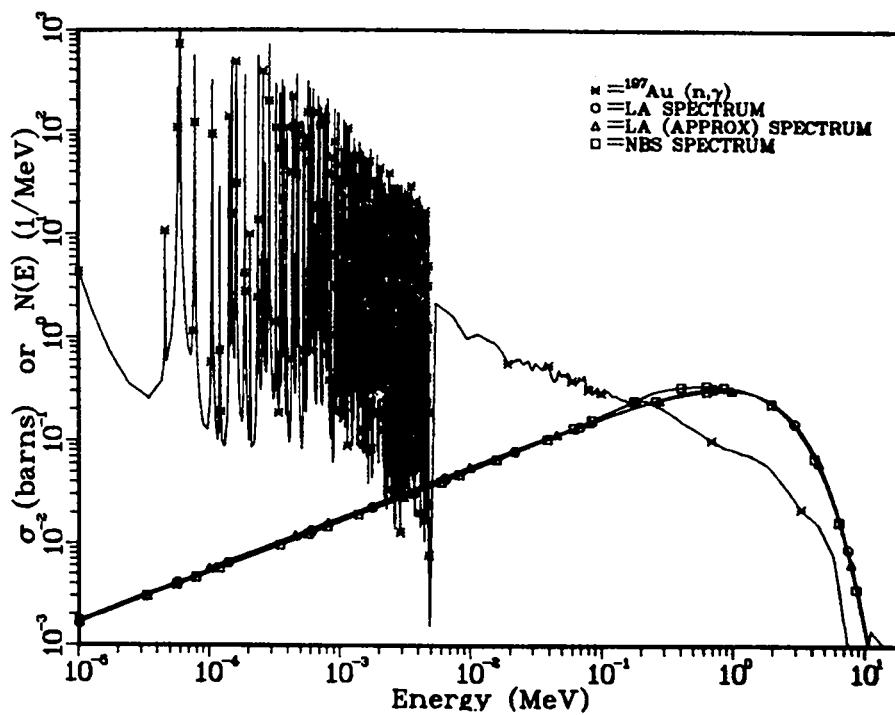


Fig. 21.
 The $^{197}\text{Au}(n,\gamma)$ cross section compared with three representations of the ^{252}Cf s.f. spectrum.

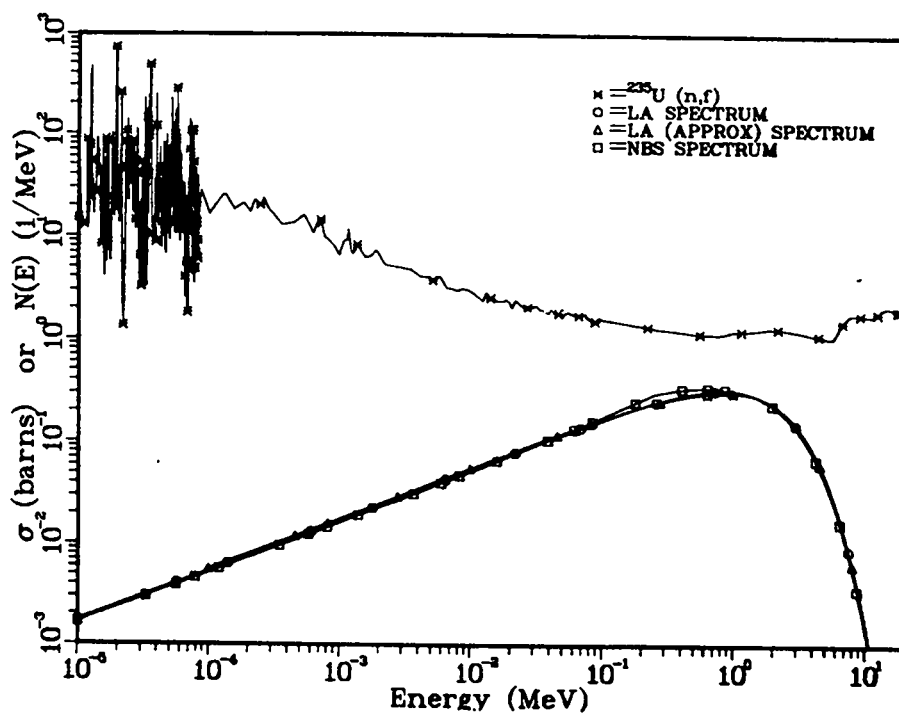


Fig. 22.
 The $^{235}\text{U}(n,f)$ cross section compared with three representations of the ^{252}Cf s.f. spectrum.

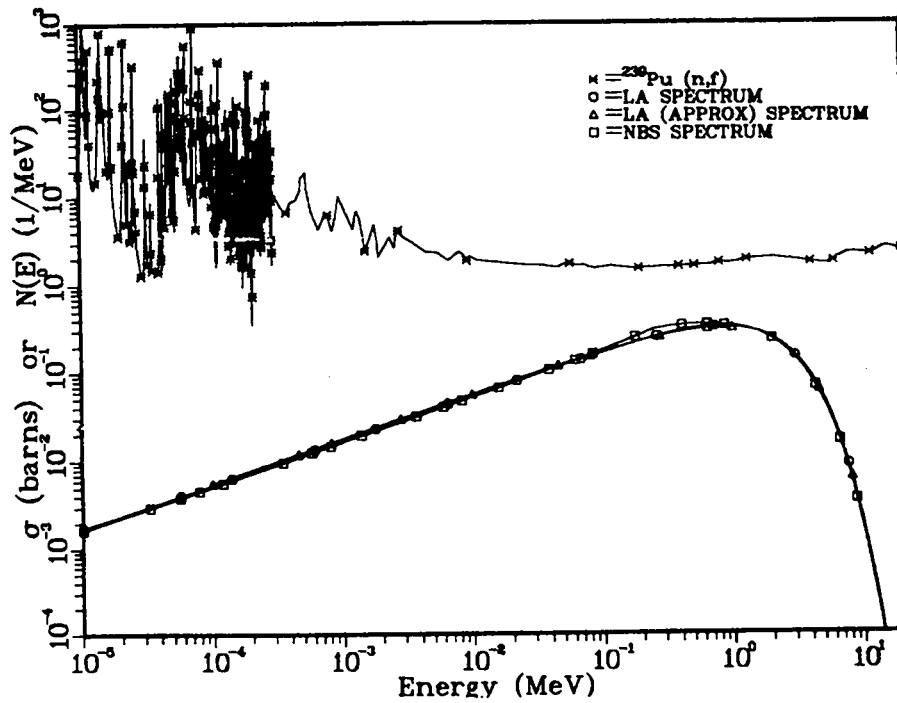


Fig. 23.
 The ${}^{239}\text{Pu}(n,f)$ cross section compared with three representations of the ${}^{252}\text{Cf}$ s.f. spectrum.

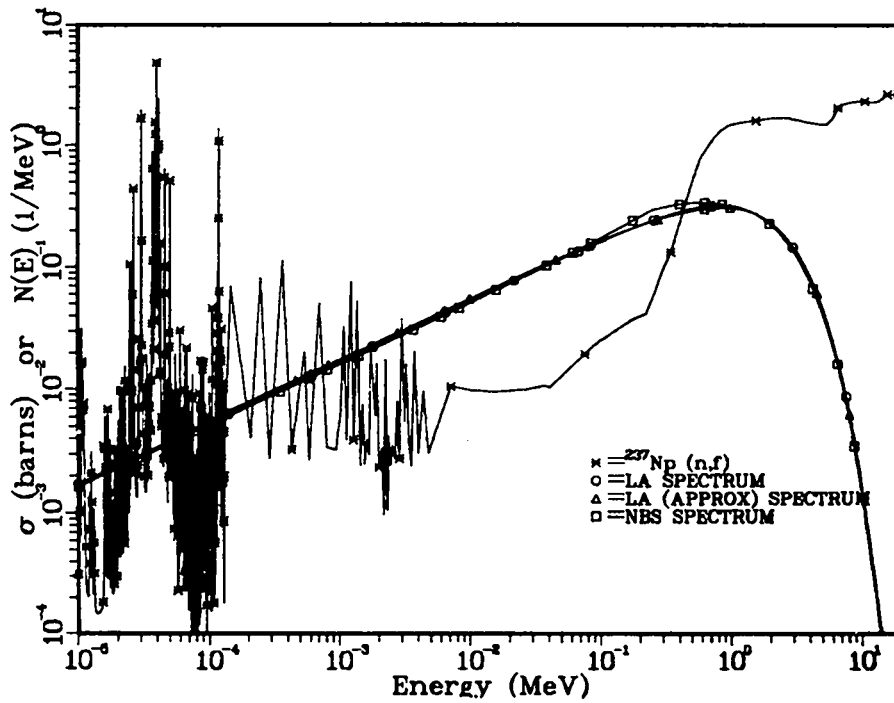


Fig. 24.
 The ${}^{237}\text{Np}(n,f)$ cross section compared with three representations of the ${}^{252}\text{Cf}$ s.f. spectrum.

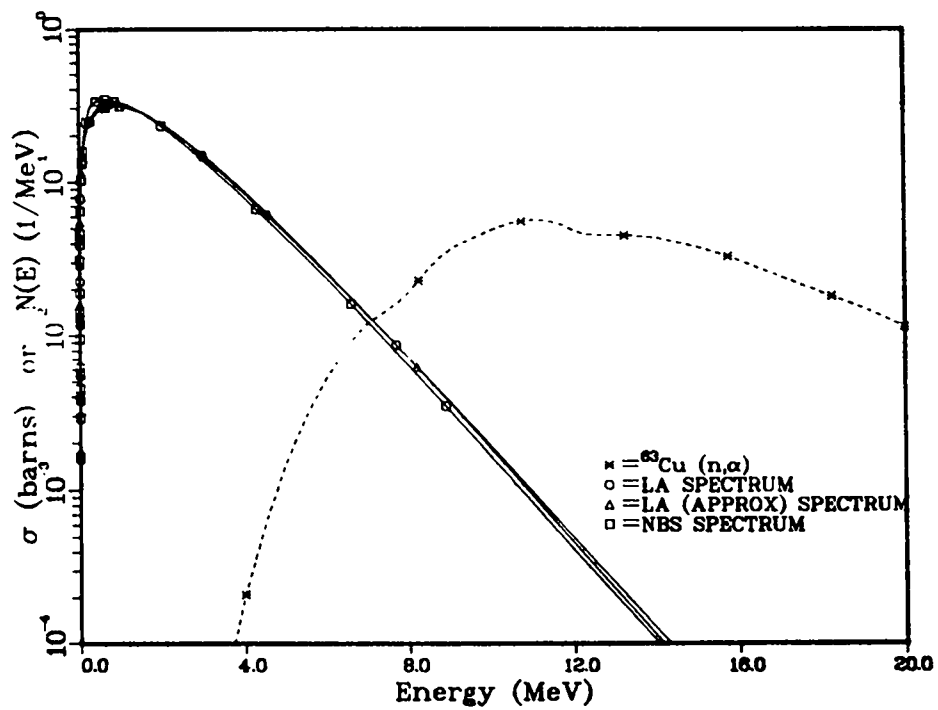


Fig. 25.

Comparison of the $^{63}\text{Cu}(n,\alpha)$ cross section with three representations of the ^{252}Cf s.f. spectrum.

The Doppler broadening module was also modified for vector processing and a faster calculation of the complementary error function was installed. It has long been known that BROADR destroys the infinitely dilute unresolved cross sections on the RECONR PENDF tape. This has not been a serious problem because these numbers were not used in the multigroup calculation. However, they do appear in the ACE library used by the MCNP continuous-energy MONTE-CARLO code. To correct this small error, UNRESR has been modified to replace the unresolved cross sections on the BROADR PENDF with corrected values.

Another change related to unresolved cross sections was made in GROUPT. The GETUNR routine now interpolates in the table of unresolved shielding factors to find the σ_0 values requested in the GROUPT input. This means that the σ_0 grid used in GROUPT can be different from that used in UNRESR. This feature would normally be used to insert additional σ_0 values (for example, 50 b for ^{238}U) in GROUPT for cases where the resolved range is especially important and in which the self-shielding effects in the resolved range are very large.

The nuclear heating and radiation damage calculations in HEATR now include the momentum-balance correction to capture recoil described in the last quarterly report. Because total energy is no longer conserved with this change, a diagnostic message has been provided to compare the total energy available to the capture photon spectrum with the Q-value for the capture reaction. If this difference is not negligible, the user would expect to see errors in heating in large systems, although the results for small systems would be better than those given by the older energy-balance method. As has been pointed out before,⁴² the best solution to this problem is to improve the evaluations.

The specifications of input and output units have been changed to make future conversions to the FORTRAN-77 standard easier by adding local calls to open (OPENZ) and close (CLOSZ) input and output files. These subroutines can easily be modified to use the standard OPEN and CLOSE calls as they become more available around the world. This change also reduces conflicts found on some systems when the same "unit" is used for formatted and binary input and output in different parts of the NJOY run.

III. FISSION PRODUCTS AND ACTINIDES: YIELDS, DECAY DATA, DEPLETION, AND BUILDUP

A. Comparisons of Aggregate ^{235}U and ^{239}Pu Fission-Product β^- and γ Decay Energies with Summation Calculations Based on Recent Libraries (T. R. England, R. J. LaBauve, W. B. Wilson, D. C. George, and N. L. Whittemore)

Recent evaluated data libraries in the USA (ENDF/B-V),⁴³ Japan (JNDC--October 1980 Version),⁴⁴ and the UK (UKFPDD-2)⁴⁵ have incorporated extensive experimentally measured decay energies along with improved yields, branching fractions, half-lives, and cross sections. The major USA library, ENDF/B-V, incorporates more detailed spectra and contains $\approx 70\%$ more nuclides having experimentally derived decay energies than did ENDF/B-IV.⁴⁶ Figure 26 shows the aggregate experimental decay energy fractions vs time for a ^{235}U fission pulse. Values are four to five times larger than those of ENDF/B-IV at 0.1 s cooling.

These three independently evaluated libraries⁴³⁻⁴⁵ show a common discrepancy when used in summation calculations and compared with results of aggregate decay power experiments. At short cooling times, the γ decay power is generally too small and the β^- decay power is generally too large. This is illustrated in Figs. 27 and 28 using the Dickens et al. integral experiments at Oak Ridge National Laboratory^{47,48} as a basis for comparison. Other comparisons have been made; in particular, Journey's gamma measurements⁴⁹ at Los Alamos show good agreement with calculations, including the time range 10^3 - 10^4 s where the Dickens data for ^{235}U are smaller than calculations using these libraries. However, as noted in the next section of this report, the Dickens and Journey experimental gamma decay data are remarkably consistent for most time intervals.

The experimental data in these plots are reduced to values equivalent to a fission pulse using the method described by Dickens in Ref. 47. For cooling times comparable to, or shorter than, the experimental irradiation period, a more accurate method (for example, Ref. 50) is required; this was needed in the comparisons made with the Los Alamos experiments following 20 000-s irradiation periods. Results are given in the next section of this report.

One can, of course, compare the calculated decay energies following the actual irradiation times. Figures 29-34 show aggregate ^{235}U and ^{239}Pu beta and gamma component energies using ENDF/B-IV and -V and compare with the Dickens' measurements for the three irradiation times he used. Earlier progress reports have shown similar comparisons with Los Alamos measurements.

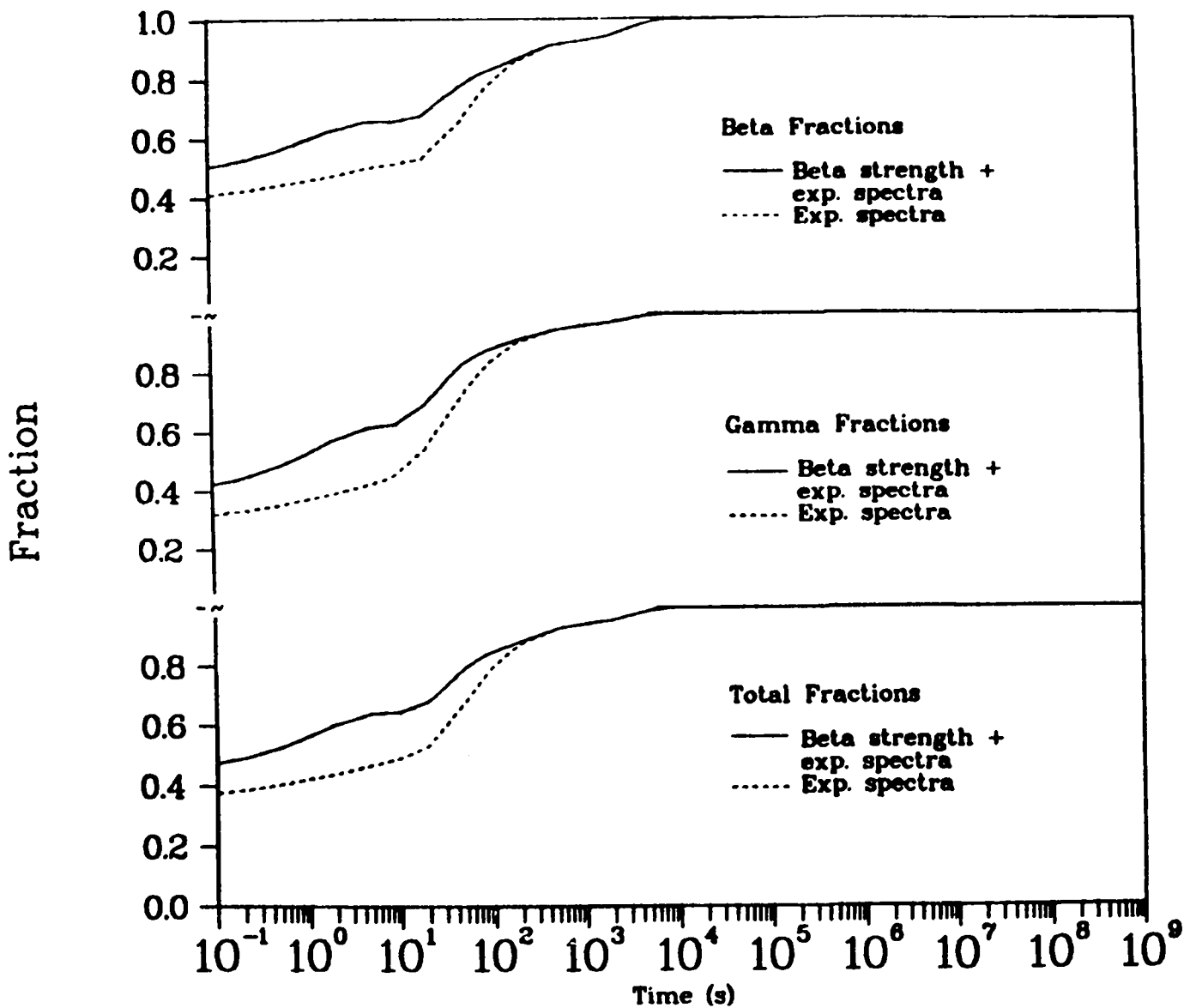


Fig. 26.
 ^{235}U thermal fission pulse: Fractional energies from experimental data in ENDF/B-V.

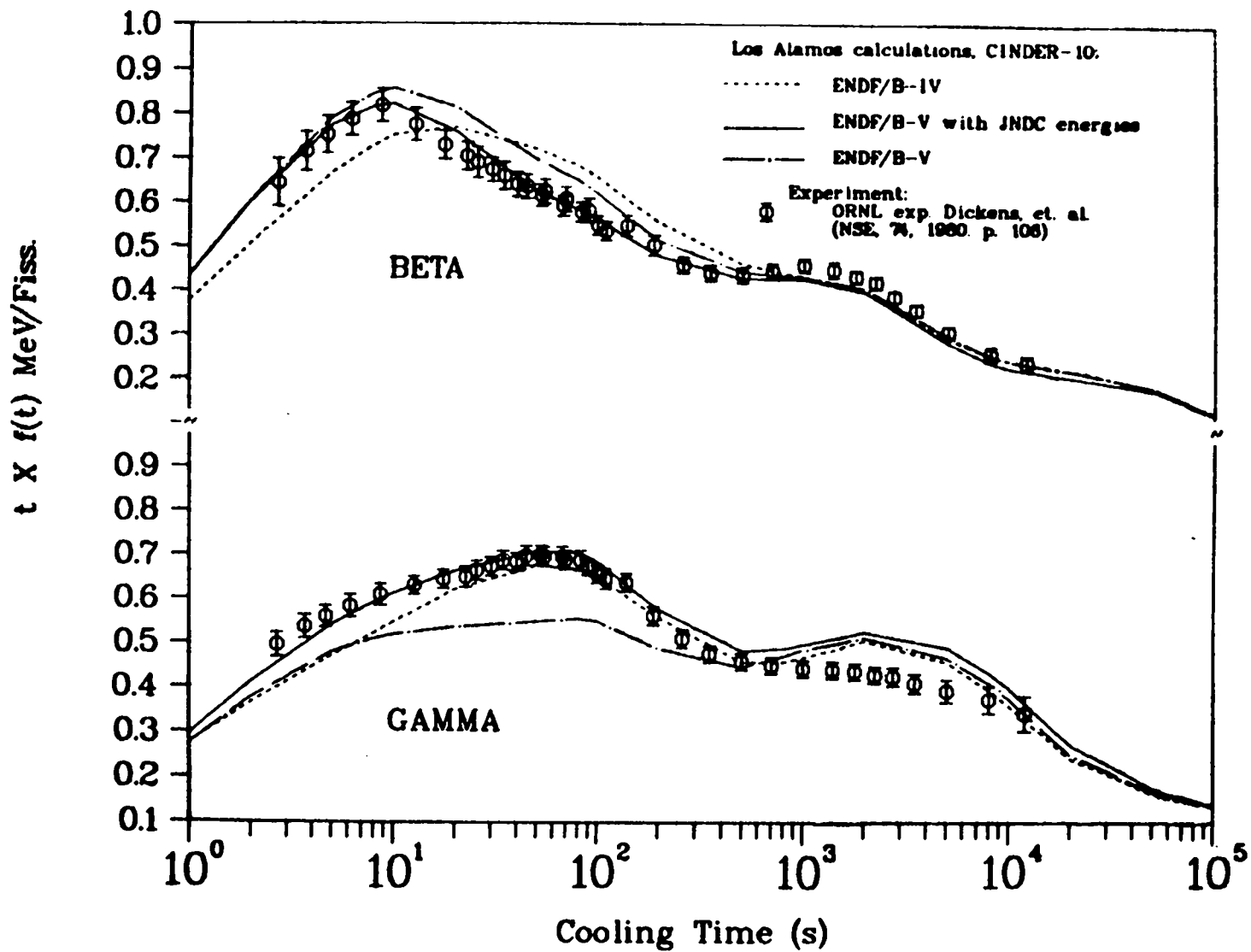


Fig. 27

^{235}U thermal fission pulse comparisons.

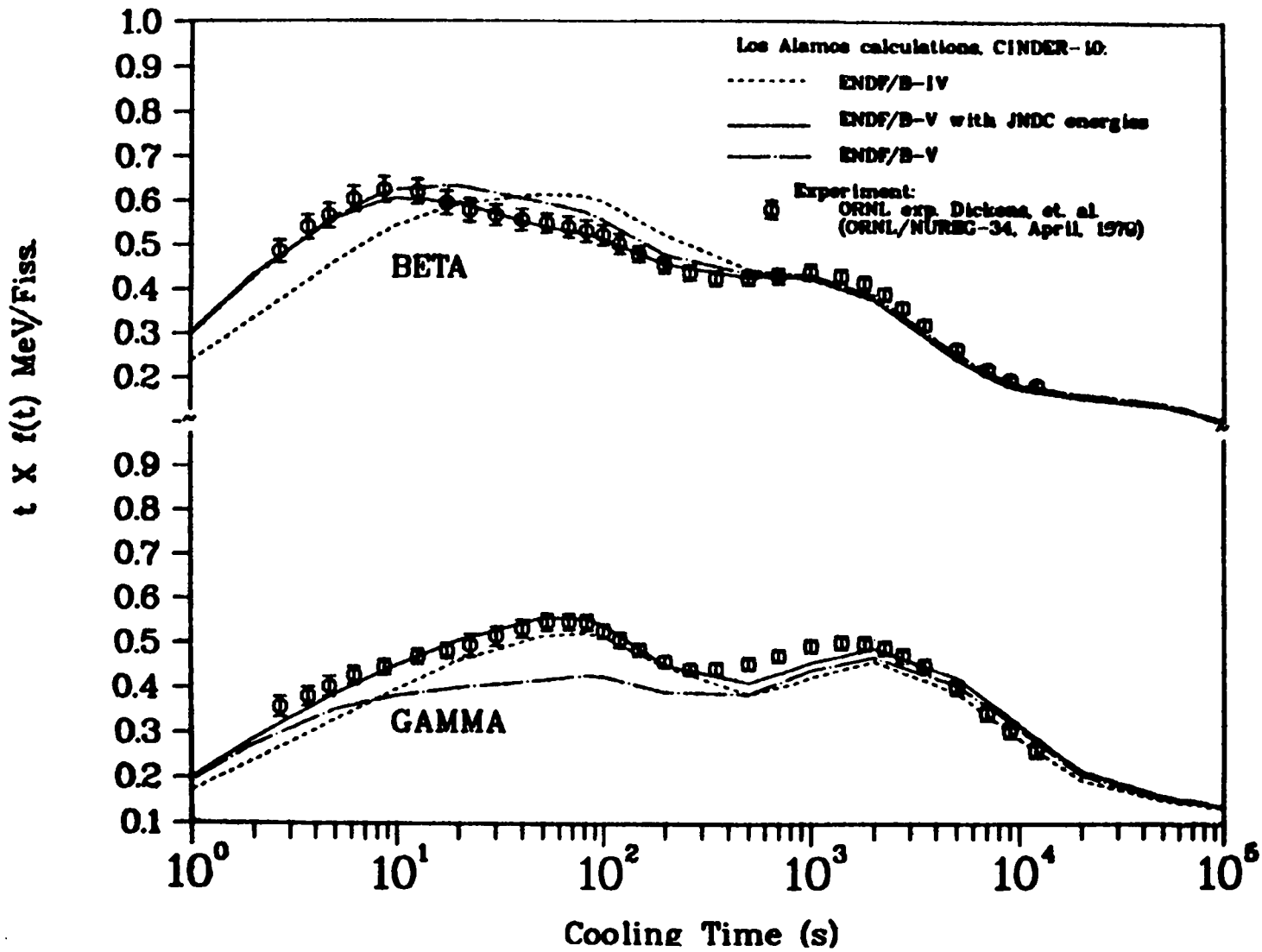


Fig. 28.

²³⁹Pu thermal fission pulse comparisons.

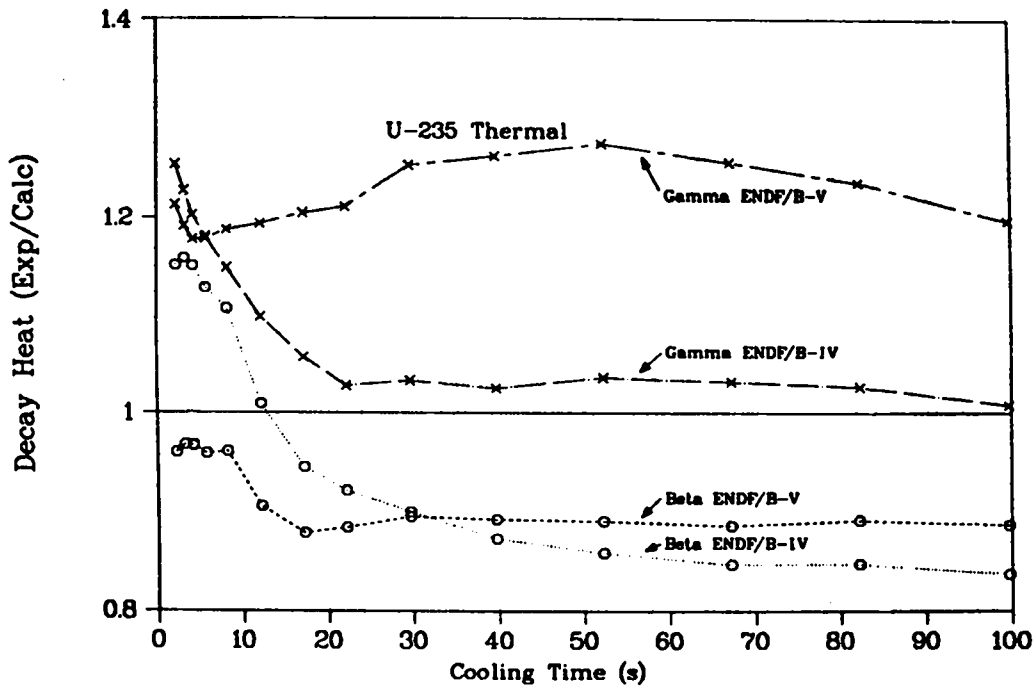


Fig. 29.
 Ratio of experimental to calculated decay heat
 for a 1-s irradiation at constant flux. (Ex-
 perimental data from NSE 74, 1980, p. 106).

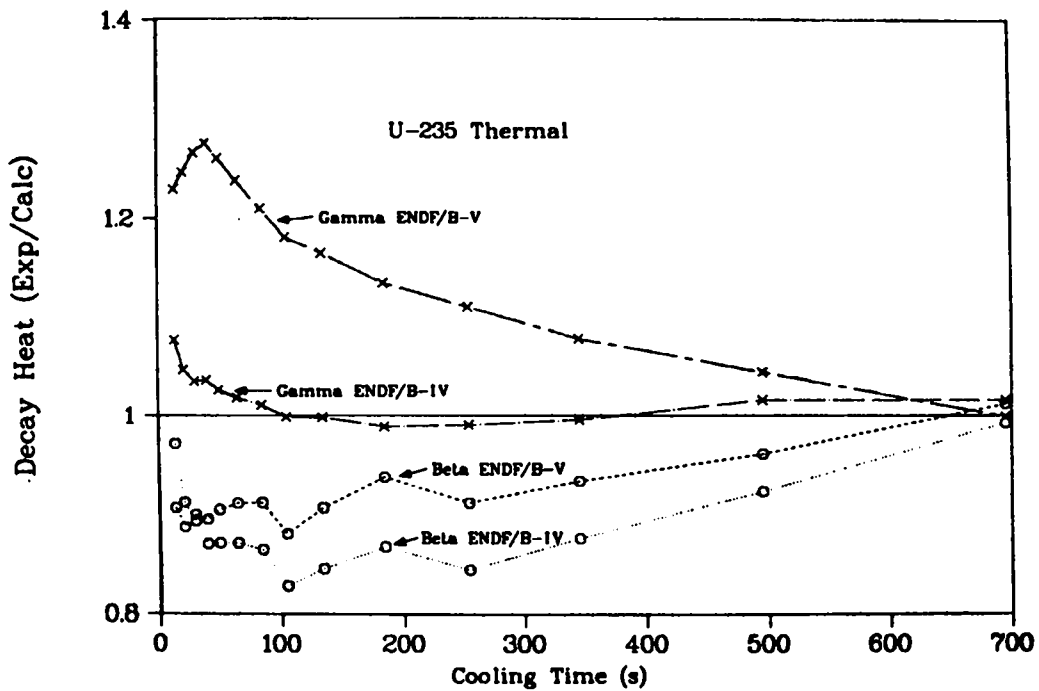


Fig. 30.
 Ratio of experimental to calculated decay heat
 for a 10-s irradiation at constant flux. (Ex-
 perimental data from NSE 74, 1980, p. 106).

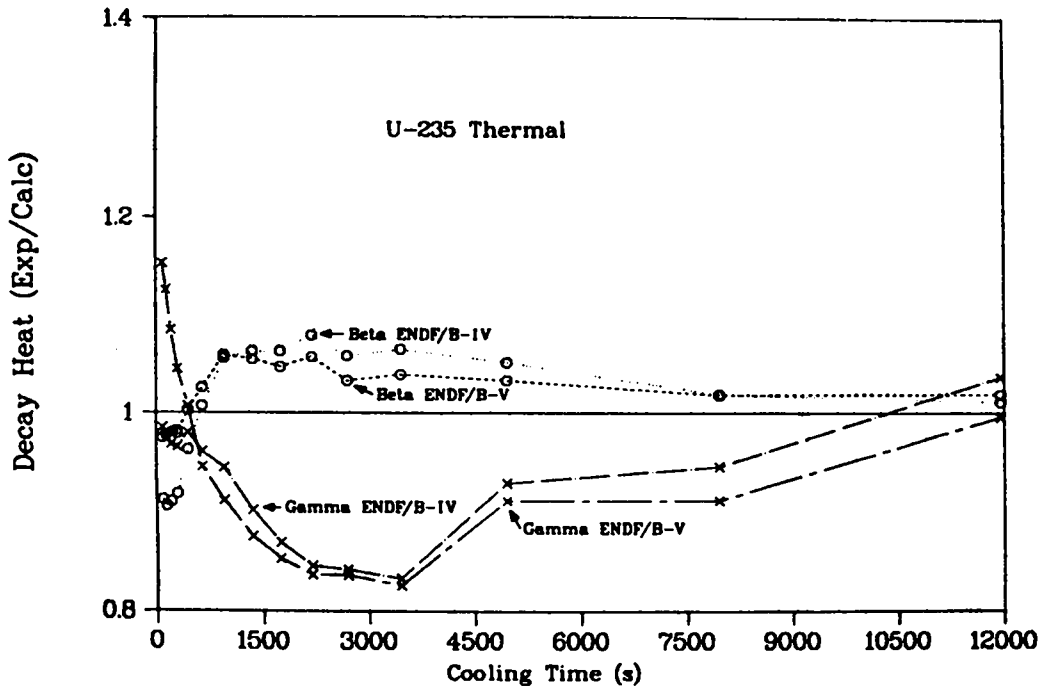


Fig. 31.
Ratio of experimental to calculated decay heat
for a 100-s irradiation at constant flux. (Ex-
perimental data from NSE 74, 1980, p. 106).

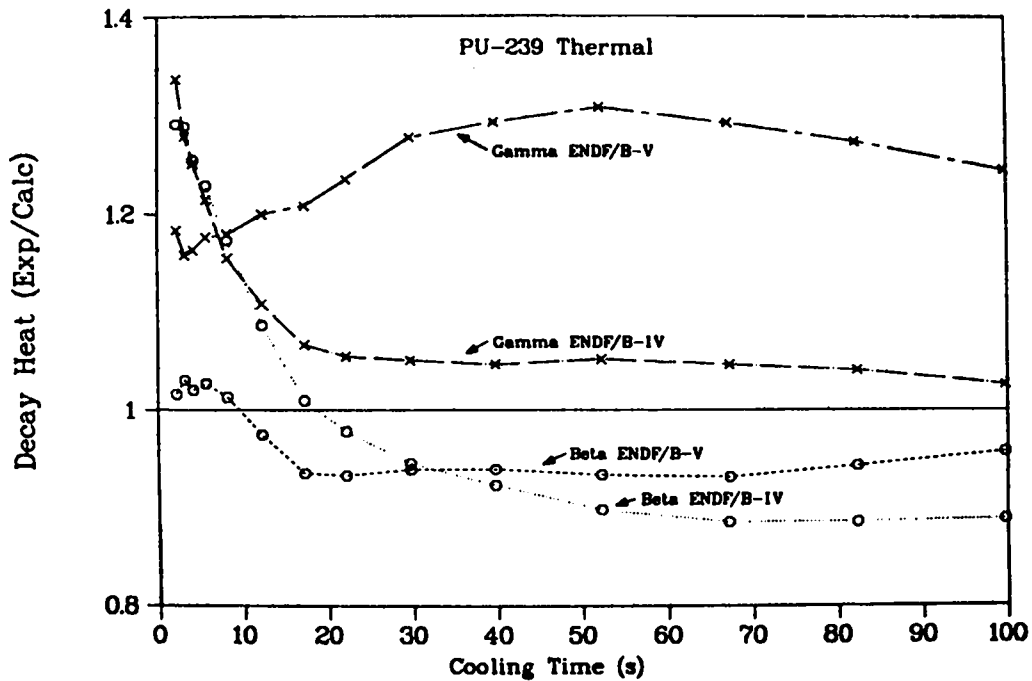


Fig. 32.
Ratio of experimental to calculated decay heat
for a 1-s irradiation at constant flux. (Ex-
perimental data from ORNL exp., Dickens, ORNL/
NUREG-34, April 1978).

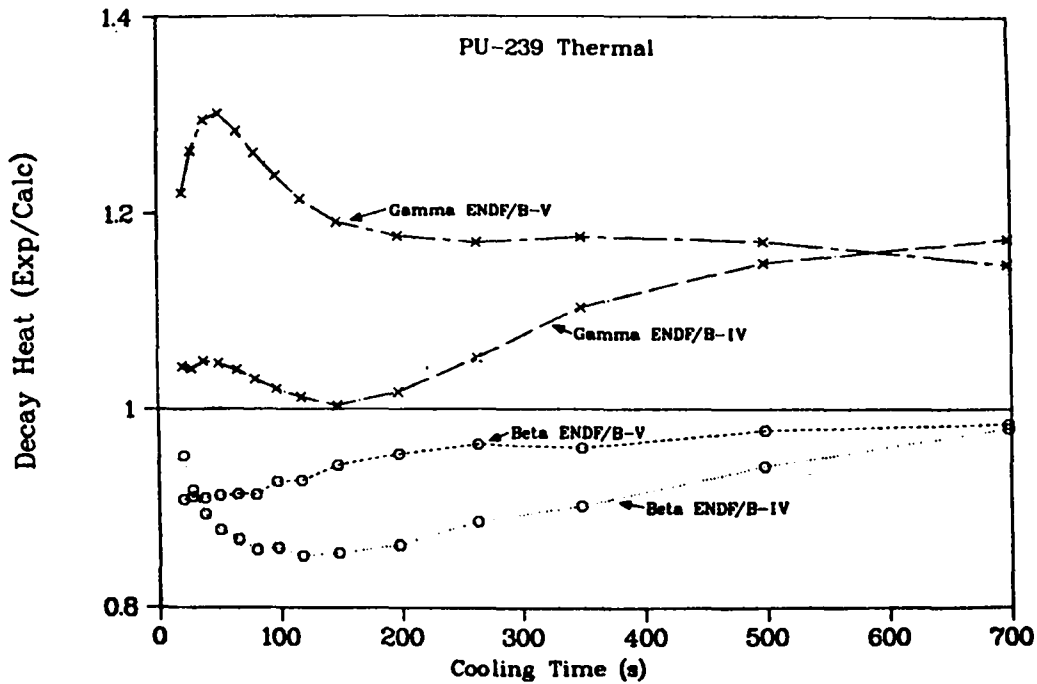


Fig. 33.

Ratio of experimental to calculated decay heat for a 5-s irradiation at constant flux. (Experimental data from ORNL exp., Dickens, ORNL/NUREG-34, April 1978).

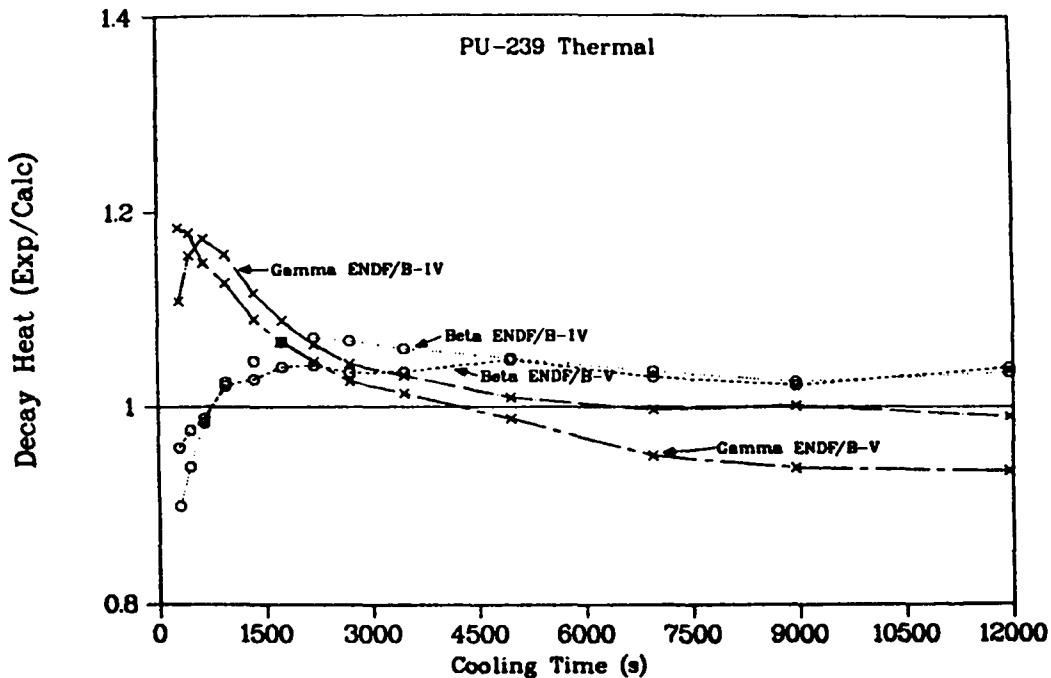


Fig. 34.

Ratio of experimental to calculated decay heat for a 100-s irradiation at constant flux. (Experimental data from ORNL exp., Dickens, ORNL/NUREG-34, April 1978).

Very few errors (none that are significant to the aggregate decay power) have been found in the ENDF/B-V files. The CINDER-10 code library⁵¹ based on processing these files has been extensively checked for errors, and pulse calculations have been independently verified.⁵²

Based on the results in Figs. 27 and 28 for the two fuels differing greatly in mass chain yields and isotopic distributions, one is forced to conclude that differences are probably due to decay energies. In particular, the evaluated experimental energies of individual nuclides, because of their dominance in the aggregate calculations (Fig. 26), are likely deficient for some nuclides. This has been a long-standing speculation,⁵³ and the same speculation, based on similar comparisons, has been noted in recent work.^{44, 45, 54} The spectral comparisons briefly noted in the next section strongly support the speculation.

The need to supplement some of the experimental energies of the individual nuclides with a model calculation has already been assumed in compiling the 1981 Japanese data file⁵⁵ in which they note "...that the complex beta-decay schemes based on gamma-ray peak analysis and intensity balance should be regarded as doubtful from the viewpoint of completeness." For nuclides having Q-values >5 MeV, they used fitted parameters in a model based on the gross theory of beta decay to replace β^- and γ experimental energies. In Figs. 27 and 28, we have used the JNDC energies with, otherwise, all ENDF/B-V decay parameters. The improved agreement with these sensitive pulse cases for two fuels differing greatly in fission-yield distributions is remarkable. These results strongly indicate that yield and decay parameters in ENDF/B-V, other than some decay energies of short-lived nuclides, are very good. We anticipate making an improvement in aggregate decay energies similar to the result from the JNDC file using model calculations and possibly using a recent unpublished code.⁵⁶

These total energy comparisons have even stronger implication for β^- , γ , and antineutrino (ν) spectra. In particular, the β^- and ν energies are not only smaller than previously supposed but the spectra are also softer (similarly, the gamma spectra are generally harder than would be calculated with ENDF/B-V files). The current conclusions regarding the ν mass, based largely on measured vs calculated reaction rates in the source spectra from reactors, could be strongly affected by these results.

B. Integral Data Testing of ENDF/B Fission Product Data (D. C. George, R. J. LaBauve, and T. R. England)

The data in the previous section are based on direct CINDER-10 calculations of the aggregate beta and gamma decay energies. The activities from these calculations are also being used to calculate beta and gamma spectra and to compare these spectra with experimental data. The spectral comparisons provide additional detail; the summation of these spectra should agree with the direct calculations. The comments and summed spectra in this section agree with the information in the previous section; the spectral comparisons do show that the calculated gamma spectra are generally too soft and the beta spectra generally too hard at short cooling times.

The work reported in last quarter's report,⁵⁷ comparing gamma-ray decay energies calculated using ENDF/B-IV⁵⁸ and ENDF/B-V⁵⁹ fission product data with decay energies experimentally measured,⁶⁰⁻⁶² was expanded to include beta decay energies from ^{235}U and beta and gamma decay energies from ^{239}Pu .

Two additional calculations of decay energies were performed. The first was based on fission product spectra supplied by A. Tobias⁴⁵ and is identified on the following figures as UK. The second normalized the ENDF/B-V fission product spectra to the average total energies supplied by the Japanese Atomic Energy Research Institute⁶³ and is identified as ENDF-J.

Figures 35 through 38 show typical spectral comparisons. The following observations can be made from such comparisons.

- (1) The experimental data⁶⁰⁻⁶² are consistent.
- (2) No method of calculating the decay energy spectra fits the experimental data very well.
- (3) In general, experimental gamma decay energies at short cooling times (<100 s) are low at low energies (<0.8 MeV) and high at high energies (>1.6 MeV) in comparison to calculated energies.
- (4) In general, experimental beta decay energies are high for all cooling times for low energies (<1.4 MeV) and low for high energies (>1.8 MeV).

A report describing this work is in preparation.

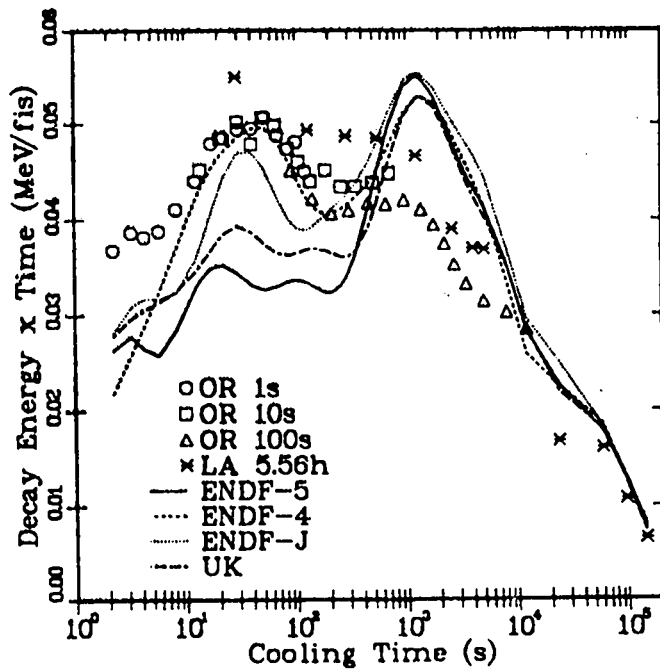


Fig. 35.
Comparison of gamma-ray decay
energy from ^{235}U (1.0 - 1.2 MeV).

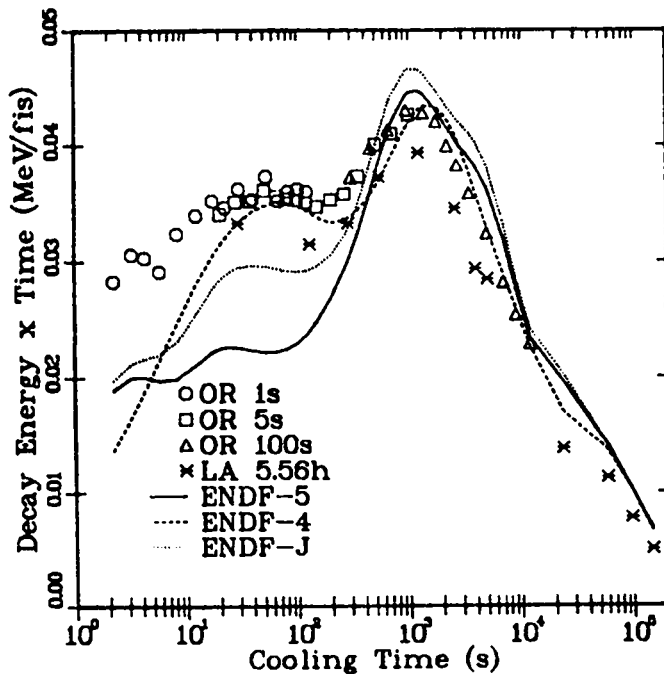


Fig. 36.
Comparison of gamma-ray decay
energy from ^{239}Pu (1.0 - 1.2 MeV).

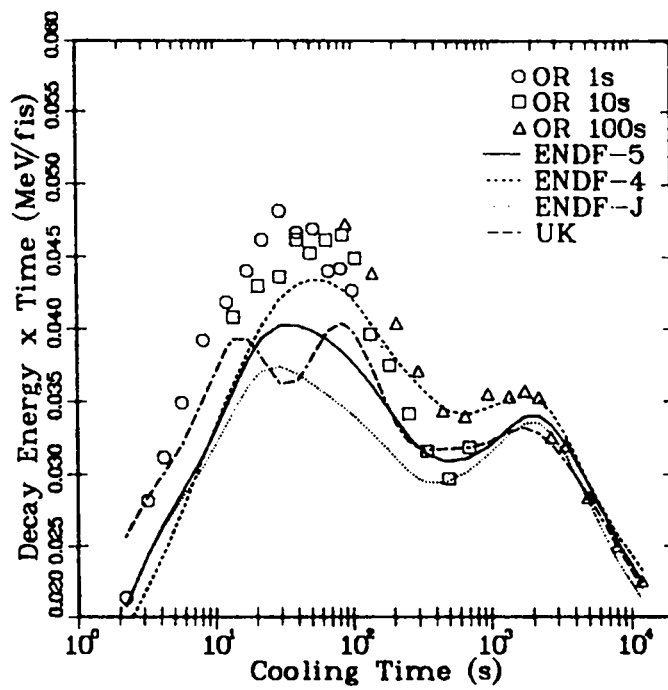


Fig. 37.

Comparison of beta-ray decay energy from ^{235}U (1.0 - 1.2 MeV).

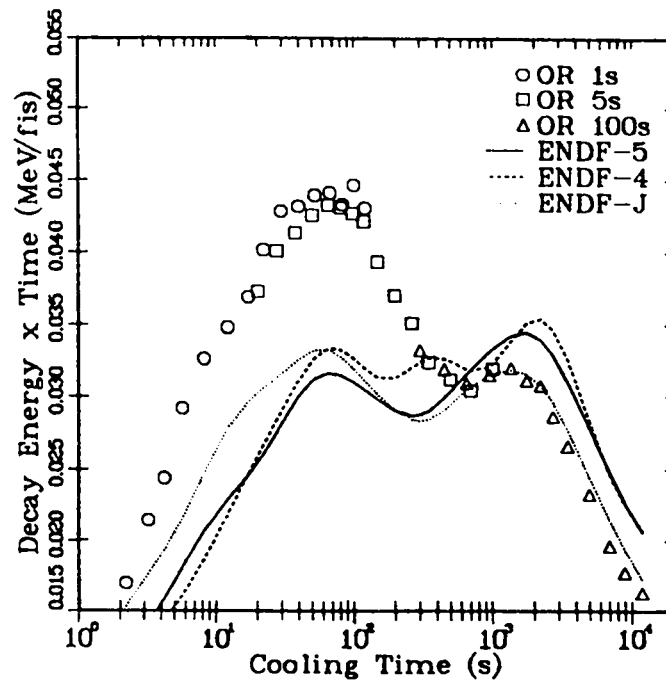


Fig. 38.

Comparison of beta-ray decay energy from ^{239}Pu (1.0 - 1.2 MeV).

C. Neutron Capture Branching Fractions (T. R. England, W. B. Wilson, and N. L. Whittemore)

In summation and depletion codes, the (n, gamma) branching fractions (describing reaction cross sections producing isomeric states) are required where there is extensive neutron capture. In ENDF/B-V the energy-dependent branching fractions are given in File 9 (MF = 9) for only three actinides and no values are given for the fission products; yet such data can be very important, particularly in thermal reactors. For example, the branching producing ^{148m}Pm from ^{147}Pm nearly doubles the amount of ^{149}Sm that would be produced from the mass 149 fission yield.

In Table VII we have listed the 196 fission products and 41 actinides having cross-section evaluations, along with Column NB identifying the number of explicit isomeric plus ground states and with approximate (n, gamma) branching values. These are not ENDF/B-V; the values have been generated using reaction cross sections from a variety of sources. Such cross sections are actually energy dependent, but this dependence is not usually known; however, when values are displayed as a branching fraction, the dependence is usually weak. We recommend the fractions in Table VII for use in summation codes. Here B1, B2, B3 refer to the branching to the ground, first and second isomeric states, respectively.

D. ENDF/B-V Reference Data Report [T. R. England, W. B. Wilson, R. E. Schenter (Hanford Engineering Development Lab.), and N. L. Whittemore]

Several minor codes have been completed and used to process, abstract, and prepare a final listing of the major decay and yield parameters for the 877 fission products and 60 actinides in ENDF/B-V Mod "O." This extensive listing of completed data is the primary part of a final reference document.⁶⁴ The recently completed cross-section tables and (n, gamma) cross sections (described in the previous two sections), as well as mass chain yields, complete all necessary tabular data for the final report. The intent is to provide the general user with a single, compact desk document listing the most often requested data.

TABLE VII
APPROXIMATE (N.GAMMA) BRANCHING FRACTIONS*

NUCLIDE S	ID NB		BRANCHING V5 FRACTIONS			NUCLIDE S	ID NB		BRANCHING V5 FRACTIONS		
			B1	B2	B3				B1	B2	B3
			32-GE- 72 0	320720	2				0.968	0.032	0.000
32-GE- 73 0	320730	1	1.000	0.000	0.000	40-ZR- 96 0	400960	1	1.000	0.000	0.000
32-GE- 74 0	320740	2	0.656	0.344	0.000	42-MO- 96 0	420960	1	1.000	0.000	0.000
34-SE- 74 0	340740	1	1.000	0.000	0.000	44-RU- 96 0	440960	1	1.000	0.000	0.000
33-AS- 75 0	330750	1	1.000	0.000	0.000	42-MO- 97 0	420970	1	1.000	0.000	0.000
32-GE- 76 0	320760	2	0.460	0.540	0.000	42-MO- 98 0	420980	1	1.000	0.000	0.000
34-SE- 76 0	340760	2	0.730	0.264	0.000	44-RU- 98 0	440980	1	1.000	0.000	0.000
34-SE- 77 0	340770	1	1.000	0.000	0.000	42-MO- 99 0	420990	1	1.000	0.000	0.000
34-SE- 78 0	340780	2	0.259	0.741	0.000	43-TC- 99 0	430990	1	1.000	0.000	0.000
36-KR- 78 0	360780	2	0.955	0.045	0.000	44-RU- 99 0	440990	1	1.000	0.000	0.000
35-BR- 79 0	350790	2	0.743	0.257	0.000	42-MO-100 0	421000	1	1.000	0.000	0.000
34-SE- 80 0	340800	2	0.869	0.131	0.000	44-RU-100 0	441000	1	1.000	0.000	0.000
36-KR- 80 0	360800	2	0.635	0.365	0.000	44-RU-101 0	441010	1	1.000	0.000	0.000
35-BR- 81 0	350810	2	0.149	0.851	0.000	44-RU-102 0	441020	1	1.000	0.000	0.000
34-SE- 82 0	340820	2	0.129	0.871	0.000	46-PD-102 0	461020	1	1.000	0.000	0.000
36-KR- 82 0	360820	2	0.556	0.444	0.000	44-RU-103 0	441030	1	1.000	0.000	0.000
36-KR- 83 0	360830	1	1.000	0.000	0.000	45-RH-103 0	451030	2	0.908	0.092	0.000
36-KR- 84 0	360840	2	0.318	0.682	0.000	44-RU-104 0	441040	1	1.000	0.000	0.000
38-SR- 84 0	380840	2	0.359	0.641	0.000	46-PD-104 0	461040	1	1.000	0.000	0.000
36-KR- 85 0	360850	1	1.000	0.000	0.000	44-RU-105 0	441050	1	1.000	0.000	0.000
37-RB- 85 0	370850	2	0.891	0.109	0.000	45-RH-105 0	451050	2	0.688	0.312	0.000
36-KR- 86 0	360860	1	1.000	0.000	0.000	46-PD-105 0	461050	1	1.000	0.000	0.000
37-RB- 86 0	370860	1	1.000	0.000	0.000	44-RU-106 0	441060	1	1.000	0.000	0.000
38-SR- 86 0	380860	2	0.704	0.296	0.000	46-PD-106 0	461060	2	0.884	0.116	0.000
37-RB- 87 0	370870	1	1.000	0.000	0.000	48-CD-106 0	481060	1	1.000	0.000	0.000
38-SR- 87 0	380870	1	1.000	0.000	0.000	46-PD-107 0	461070	1	1.000	0.000	0.000
38-SR- 88 0	380880	1	1.000	0.000	0.000	47-AG-107 0	471070	2	0.950	0.050	0.000
38-SR- 89 0	380890	1	1.000	0.000	0.000	46-PD-108 0	461080	2	0.984	0.016	0.000
39- Y- 89 0	390890	2	0.999	0.001	0.000	48-CD-108 0	481080	1	1.000	0.000	0.000
38-SR- 90 0	380900	1	1.000	0.000	0.000	47-AG-109 0	471090	2	0.950	0.050	0.000
39- Y- 90 0	390900	2	0.500	0.500	0.000	46-PD-110 0	461100	2	0.913	0.087	0.000
40-ZR- 90 0	400900	1	1.000	0.000	0.000	48-CD-110 0	481100	2	0.969	0.031	0.000
39- Y- 91 0	390910	1	1.000	0.000	0.000	47-AG-111 0	471110	1	1.000	0.000	0.000
40-ZR- 91 0	400910	1	1.000	0.000	0.000	48-CD-111 0	481110	1	1.000	0.000	0.000
40-ZR- 92 0	400920	1	1.000	0.000	0.000	48-CD-112 0	481120	2	1.000	0.000	0.000
42-MO- 92 0	420920	2	0.980	0.020	0.000	50-SN-112 0	501120	2	0.700	0.300	0.000
40-ZR- 93 0	400930	1	1.000	0.000	0.000	48-CD-113 0	481130	1	1.000	0.000	0.000
41-NB- 93 0	410930	2	1.000	0.000	0.000	49-IN-113 0	491130	2	0.328	0.672	0.000
40-ZR- 94 0	400940	1	1.000	0.000	0.000	48-CD-114 0	481140	2	0.882	0.118	0.000
41-NB- 94 0	410940	2	0.961	0.039	0.000	50-SN-114 0	501140	1	1.000	0.000	0.000
42-MO- 94 0	420940	1	1.000	0.000	0.000						
40-ZR- 95 0	400950	1	1.000	0.000	0.000						
41-NB- 95 0	410950	1	1.000	0.000	0.000						

TABLE VII
(Cont)

NUCLIDE S	ID NB		BRANCHING V5 FRACTIONS		
			B1	B2	B3
			48-CD-115 1	481151 1	1.000
49-IN-115 0	491150 3	0.223	0.322	0.455	
50-SN-115 0	501150 1	1.000	0.000	0.000	
48-CD-116 0	481160 2	0.800	0.200	0.000	
50-SN-116 0	501160 2	0.950	0.050	0.000	
50-SN-117 0	501170 1	1.000	0.000	0.000	
50-SN-118 0	501180 2	0.395	0.605	0.000	
50-SN-119 0	501190 1	1.000	0.000	0.000	
50-SN-120 0	501200 2	0.994	0.006	0.000	
52-TE-120 0	521200 2	0.870	0.130	0.000	
51-SB-121 0	511210 2	0.991	0.009	0.000	
50-SN-122 0	501220 2	0.006	0.994	0.000	
52-TE-122 0	521220 2	0.607	0.393	0.000	
50-SN-123 0	501230 1	1.000	0.000	0.000	
51-SB-123 0	511230 3	0.986	0.009	0.005	
52-TE-123 0	521230 1	1.000	0.000	0.000	
50-SN-124 0	501240 2	0.030	0.970	0.000	
51-SB-124 0	511240 1	1.000	0.000	0.000	
52-TE-124 0	521240 2	0.994	0.006	0.000	
54-XE-124 0	541240 2	0.832	0.168	0.000	
50-SN-125 0	501250 1	1.000	0.000	0.000	
51-SB-125 0	511250 3	0.500	0.250	0.250	
52-TE-125 0	521250 1	1.000	0.000	0.000	
50-SN-126 0	501260 2	0.500	0.500	0.000	
51-SB-126 0	511260 1	1.000	0.000	0.000	
52-TE-126 0	521260 2	0.874	0.126	0.000	
54-XE-126 0	541260 2	0.880	0.120	0.000	
52-TE-127 1	521271 1	1.000	0.000	0.000	
53- I-127 0	531270 1	1.000	0.000	0.000	
52-TE-128 0	521280 2	0.944	0.056	0.000	
54-XE-128 0	541280 2	0.909	0.091	0.000	
52-TE-129 1	521291 1	1.000	0.000	0.000	
53- I-129 0	531290 2	0.333	0.667	0.000	
54-XE-129 0	541290 1	1.000	0.000	0.000	
52-TE-130 0	521300 2	0.909	0.091	0.000	
53- I-130 0	531300 1	1.000	0.000	0.000	
54-XE-130 0	541300 2	0.877	0.123	0.000	
53- I-131 0	531310 2	1.000	0.000	0.000	
54-XE-131 0	541310 1	1.000	0.000	0.000	
52-TE-132 0	521320 2	0.500	0.500	0.000	
54-XE-132 0	541320 2	0.900	0.100	0.000	
54-XE-133 0	541330 2	1.000	0.000	0.000	

NUCLIDE S	ID NB		BRANCHING V5 FRACTIONS		
			B1	B2	B3
			55-CS-133 0	551330 2	0.924
54-XE-134 0	541340 2	0.988	0.012	0.000	
55-CS-134 0	551340 2	1.000	0.000	0.000	
56-BA-134 0	561340 2	0.926	0.074	0.000	
53- I-135 0	531350 2	0.500	0.500	0.000	
54-XE-135 0	541350 1	1.000	0.000	0.000	
55-CS-135 0	551350 2	1.000	0.000	0.000	
56-BA-135 0	561350 2	0.995	0.005	0.000	
54-XE-136 0	541360 1	1.000	0.000	0.000	
55-CS-136 0	551360 1	1.000	0.000	0.000	
56-BA-136 0	561360 2	0.976	0.024	0.000	
55-CS-137 0	551370 2	1.000	0.000	0.000	
56-BA-137 0	561370 1	1.000	0.000	0.000	
56-BA-138 0	561380 1	1.000	0.000	0.000	
57-LA-139 0	571390 1	1.000	0.000	0.000	
56-BA-140 0	561400 1	1.000	0.000	0.000	
57-LA-140 0	571400 1	1.000	0.000	0.000	
58-CE-140 0	581400 1	1.000	0.000	0.000	
58-CE-141 0	581410 1	1.000	0.000	0.000	
59-PR-141 0	591410 2	0.658	0.342	0.000	
58-CE-142 0	581420 1	1.000	0.000	0.000	
59-PR-142 0	591420 1	1.000	0.000	0.000	
60-ND-142 0	601420 1	1.000	0.000	0.000	
58-CE-143 0	581430 1	1.000	0.000	0.000	
59-PR-143 0	591430 2	1.000	0.000	0.000	
60-ND-143 0	601430 1	1.000	0.000	0.000	
58-CE-144 0	581440 1	1.000	0.000	0.000	
60-ND-144 0	601440 1	1.000	0.000	0.000	
62-SM-144 0	621440 1	1.000	0.000	0.000	
60-ND-145 0	601450 1	1.000	0.000	0.000	
60-ND-146 0	601460 1	1.000	0.000	0.000	
60-ND-147 0	601470 1	1.000	0.000	0.000	
61-PM-147 0	611470 2	0.530	0.470	0.000	
62-SM-147 0	621470 1	1.000	0.000	0.000	
60-ND-148 0	601480 1	1.000	0.000	0.000	
61-PM-148 0	611480 1	1.000	0.000	0.000	
61-PM-148 1	611481 1	1.000	0.000	0.000	
62-SM-148 0	621480 1	1.000	0.000	0.000	
61-PM-149 0	611490 1	1.000	0.000	0.000	
62-SM-149 0	621490 1	1.000	0.000	0.000	
60-ND-150 0	601500 1	1.000	0.000	0.000	
62-SM-150 0	621500 1	1.000	0.000	0.000	
61-PM-151 0	611510 3	1.000	0.000	0.000	
62-SM-151 0	621510 1	1.000	0.000	0.000	
63-EU-151 0	631510 3	0.6519	0.3477	0.0004	

TABLE VII
(Cont)

NUCLIDE S	ID	NB	BRANCHING V5 FRACTIONS		
			B1	B2	B3
62-SM-152 O	621520	1	1.000	0.000	0.000
63-EU-152 O	631520	1	1.000	0.000	0.000
64-GD-152 O	641520	1	1.000	0.000	0.000
62-SM-153 O	621530	1	1.000	0.000	0.000
63-EU-153 O	631530	2	1.000	0.000	0.000
62-SM-154 O	621540	1	1.000	0.000	0.000
63-EU-154 O	631540	1	1.000	0.000	0.000
64-GD-154 O	641540	1	1.000	0.000	0.000
63-EU-155 O	631550	1	1.000	0.000	0.000
64-GD-155 O	641550	1	1.000	0.000	0.000
63-EU-156 O	631560	1	1.000	0.000	0.000
64-GD-156 O	641560	1	1.000	0.000	0.000
63-EU-157 O	631570	1	1.000	0.000	0.000
64-GD-157 O	641570	1	1.000	0.000	0.000
64-GD-158 O	641580	1	1.000	0.000	0.000
65-TB-159 O	651590	1	1.000	0.000	0.000
64-GD-160 O	641600	1	1.000	0.000	0.000
65-TB-160 O	651600	1	1.000	0.000	0.000
66-DY-160 O	661600	1	1.000	0.000	0.000
66-DY-161 O	661610	1	1.000	0.000	0.000
66-DY-162 O	661620	1	1.000	0.000	0.000
66-DY-163 O	661630	1	1.000	0.000	0.000
66-DY-164 O	661640	2	0.588	0.412	0.000
67-HO-165 O	671650	2	0.942	0.058	0.000
68-ER-166 O	681660	2	0.250	0.750	0.000
68-ER-167 O	681670	1	1.000	0.000	0.000
90-TH-230 O	902300	1	1.000	0.000	0.000
91-PA-231 O	912310	1	1.000	0.000	0.000
90-TH-232 O	902320	1	1.000	0.000	0.000
92- U-232 O	922320	1	1.000	0.000	0.000
91-PA-233 O	912330	1	0.101	0.899	0.000
92- U-233 O	922330	1	1.000	0.000	0.000
92- U-234 O	922340	1	1.000	0.000	0.000
92- U-235 O	922350	1	1.000	0.000	0.000
92- U-236 O	922360	1	1.000	0.000	0.000
94-PU-236 O	942360	1	1.000	0.000	0.000
92- U-237 O	922370	1	1.000	0.000	0.000
93-NP-237 O	932370	1	1.000	0.000	0.000
94-PU-237 O	942370	1	1.000	0.000	0.000
92- U-238 O	922380	1	1.000	0.000	0.000

NUCLIDE S	ID	NB	BRANCHING V5 FRACTIONS		
			B1	B2	B3
93-NP-238 O	932380	1	1.000	0.000	0.000
93-NP-239 O	932390	2	0.400	0.600	0.000
94-PU-238 O	942380	1	1.000	0.000	0.000
94-PU-239 O	942390	1	1.000	0.000	0.000
94-PU-240 O	942400	1	1.000	0.000	0.000
94-PU-241 O	942410	1	1.000	0.000	0.000
95-AM-241 O	952410	2	0.885	0.115	0.000
96-CM-241 O	962410	1	1.000	0.000	0.000
94-PU-242 O	942420	1	1.000	0.000	0.000
95-AM-242 1	952421	1	1.000	0.000	0.000
95-AM-242 O	952420	1	1.000	0.000	0.000
96-CM-242 O	962420	1	1.000	0.000	0.000
94-PU-243 O	942430	1	1.000	0.000	0.000
95-AM-243 O	952430	2	0.060	0.940	0.000
96-CM-243 O	962430	1	1.000	0.000	0.000
94-PU-244 O	942440	1	1.000	0.000	0.000
96-CM-244 O	962440	1	1.000	0.000	0.000
96-CM-245 O	962450	1	1.000	0.000	0.000
96-CM-246 O	962460	1	1.000	0.000	0.000
96-CM-247 O	962470	1	1.000	0.000	0.000
96-CM-248 O	962480	1	1.000	0.000	0.000
97-BK-249 O	972490	1	1.000	0.000	0.000
98-CF-249 O	982490	1	1.000	0.000	0.000
98-CF-250 O	982500	1	1.000	0.000	0.000
98-CF-251 O	982510	1	1.000	0.000	0.000
98-CF-252 O	982520	1	1.000	0.000	0.000
98-CF-253 O	982530	1	1.000	0.000	0.000
99-ES-253 O	992530	1	0.553	0.447	0.000

*NB=NUMBER OF (N,GAMMA) BRANCHINGS REQUIRED FOR EACH NUCLIDE.

S=ISOMERIC STATE WHERE 0=GROUND
1=FIRST ISOMERIC, ETC.

ID=10000*Z+1000*A+S.

E. Neutron Production in UO_2F_2 from the Spontaneous-Fission and Alpha Decay of U Nuclides and Subsequent $^{17,18}O(\alpha,n)$ and $^{19}F(\alpha,n)$ Reactions [W. B. Wilson, R. T. Perry (Penn. State U.), J. E. Stewart (Q-1)]

The Gas Centrifuge Enrichment Program effort within the Safeguards Assay Group (Q-1) at Los Alamos has requested the neutron source strength of UO_2F_2 , a solid reaction product of $UF_6 + H_2O$ that may be deposited within an enrichment process. Alphas emitted from $^{234-238}U$ decay are in the initial energy range $4.04 \text{ MeV} \leq E_\alpha \leq 4.77 \text{ MeV}$ and have a short range assumed much smaller than the dimensions of a UO_2F_2 deposit. The (α,n) neutron source may then be described by the thick target neutron production function

$$P(E) = \sum_{i=1}^I \left(\frac{N_i}{N} \right) \int_0^E \alpha \frac{\sigma_i(E)}{\epsilon(E)} dE, \quad (5)$$

where $\left(\frac{N_i}{N} \right)$ is the number density fraction of nuclide i ,

$\sigma_i(E)$ is the (α,n) cross section of nuclide i ,

and $\epsilon(E)$ is the stopping cross section of the material.

We have previously evaluated the $^{17,18}O(\alpha,n)$ cross sections⁶⁵ from available data⁶⁶⁻⁶⁹ for use in calculations of the neutron source characteristics of spent oxide fuels.⁶⁵ We have also taken the $^{19}F(\alpha,n)$ cross sections of Balakrishnan⁷⁰ to describe the neutron source properties of UF_6 .⁷¹ These earlier calculations required functional expressions for the stopping cross sections $\epsilon(E)$ for solid O, F, and U; these may be combined to form the stopping cross section using the Bragg-Kleeman approximation⁷²

$$\epsilon(E) = \sum_{j=1}^J \frac{N_j}{N} \epsilon_j(E), \quad (6)$$

where $\frac{N_j}{N}$ is the number density fraction of element j

and ϵ_j is the stopping cross section of element j .

All required ^{17}O , $^{18}\text{O}(\alpha, n)$ and $^{19}\text{F}(\alpha, n)$ cross-section data and O, F, and U stopping cross-section functions are given in Refs. 65 and 71. These are used in Table VIII to evaluate the ^{17}O , ^{18}O , and ^{19}F contributions to $P(E_\alpha)$ at the initial energy of each alpha particle emitted from $^{234-238}\text{U}$. The decay intensities are combined with $P(E_\alpha)$ values to determine total (α, n) neutron production per U-nuclide decay. These results are then combined with the number of spontaneous-fission neutrons per decay from Ref. 65 to give the total neutron production per U-nuclide decay. Finally, these values are combined with the decay constant λ and atomic weight A of each U nuclide to determine the total neutron production rate per gram of U nuclide in UO_2 .

TABLE VIII
SPONTANEOUS-FISSION AND (α, n) NEUTRON PRODUCTION IN UO_2F_2

U Nuclide	λ (Sec ⁻¹)	E_α (MeV)	Intensity (α /Decay)	P(E_α)(neutrons/ α -Particle)				Neutrons/Decay			n/s/g U-Nuclide in UO_2F_2
				^{17}O	^{18}O	^{19}F	Total	(α, n)	S.F.*	Total	
^{234}U	8.9800-14	4.603	0.00299	6.71-10	8.01-9	6.01-7	6.10-7	1.82-9			
		4.721	0.27916	7.37-10	9.09-9	7.59-7	7.69-7	2.15-7			
		4.773	0.71785	7.65-10	9.40-9	7.96-7	8.06-7	5.78-7			
								<u>7.95-7</u>	2.17-11	7.95-7	1.84+2
^{235}U	3.1209-17	4.155	0.00899	4.90-10	4.51-9	2.90-7	2.95-7	2.65-9			
		4.218	0.05697	5.26-10	4.81-9	3.16-7	3.21-7	1.83-8			
		4.274	0.00400	5.47-10	5.28-9	3.57-7	3.63-7	1.45-9			
		4.327	0.02998	5.69-10	5.68-9	3.74-7	4.00-7	1.20-8			
		4.329	0.00210	5.70-10	5.70-9	3.96-7	4.02-7	8.45-10			
		4.363	0.00350	5.84-10	6.00-9	4.15-7	4.22-7	1.48-9			
		4.367	0.17989	5.86-10	6.04-9	4.18-7	4.25-7	7.64-8			
		4.382	0.00300	5.91-10	6.20-9	4.25-7	4.32-7	1.30-9			
		4.398	0.56966	5.96-10	6.40-9	4.34-7	4.41-7	2.51-7			
		4.417	0.03998	6.02-10	6.60-9	4.43-7	4.50-7	1.80-8			
		4.440	0.00700	6.10-10	6.81-9	4.56-7	4.63-7	3.24-9			
		4.505	0.01199	6.30-10	7.15-9	5.18-7	5.26-7	6.30-9			
		4.558	0.03698	6.47-10	7.57-9	5.53-7	5.61-7	2.08-8			
4.660	0.04596	7.03-10	8.59-9	6.84-7	6.93-7	3.19-8					
						<u>4.46-7</u>	3.74-9	4.50-7	3.60-2		
^{236}U	9.3808-16	4.333	0.00259	5.72-10	5.73-9	3.99-7	4.05-7	1.05-9			
		4.444	0.25933	6.11-10	6.85-9	4.58-7	4.65-7	1.21-7			
		4.492	0.73808	6.26-10	7.11-9	5.05-7	5.13-7	3.78-7			
								<u>5.00-7</u>	2.29-9	5.02-7	1.20+0
^{238}U	4.9159-18	4.041	0.00100	4.22-10	3.98-9	2.36-7	2.40-7	2.40-10			
		4.150	0.11488	4.87-10	4.49-9	2.88-7	2.93-7	3.37-8			
		4.199	0.88412	5.18-10	4.71-9	3.07-7	3.12-7	2.76-7			
								<u>3.10-7</u>	1.10-6	1.41-6	1.75-2

*Spontaneous-Fission values from LA-8869-MS

REFERENCES

1. E. D. Arthur, "Calculation of Neutron Cross Sections on Isotopes of Yttrium and Zirconium," Los Alamos Scientific Laboratory report LA-7789-MS (1979).
2. D. R. Sachdev, N. T. Porile, and L. Yaffe, "Reactions of ^{88}Sr with Protons of Energies 7-85 MeV," Can. J. Chem. 45, 1149 (1967).
3. E. Gadioli, E. Gadioli-Erba, and J. H. Hogan, "Preequilibrium Decay of Nuclei with $A \approx 90$ at Excitation Energies to 100 MeV," Phys. Rev. C16, 1404 (1977).
4. J. Raynal, "Optical Model and Coupled-Channel Calculations in Nuclear Physics," International Atomic Energy Agency Report, IAEA-SMR-9/8 (1970).
5. P. A. Moldauer, "Why the Hauser-Feshbach Formula Works," Phys. Rev. C11, 426 (1975).
6. P. M. Brink, thesis, Oxford University (1955), unpublished; P. Axel, "Electric Dipole Ground State Transition Width Strength Function," Phys. Rev. 126, 671 (1962).
7. S. F. Mughabghab and D. I. Garber, "Neutron Cross Sections-Resonance Parameters," Brookhaven Report BNL 325 (1973).
8. S. Joly, D. M. Drake, and L. Nilsson, "Gamma-Ray Strength Functions in ^{104}Rh , ^{170}Tm , and ^{198}Au ," Phys. Rev. C20, 2072 (1979).
9. A. Gilbert and A. G. W. Cameron, "A Composite Nuclear-Level Density Formula with Shell Corrections," Can. J. Phys. 43, 1446 (1965).
10. C. L. Dunford, "A Unified Model for Analysis of Compound Nucleus Reactions," Atomics International Report AI-AEC-12931 (1970).
11. D. L. Hill and J. A. Wheeler, "Nuclear Constitution and the Interpretation of Fission Phenomena," Phys. Rev. 89, 1102 (1953).
12. E. D. Arthur, "Determination of Deformed Optical Model Parameters for Neutron Reactions on ^{235}U and ^{239}Pu ," in "Applied Nuclear Data Research and Development January 1-March 31, 1981," C.I. Baxman and P. G. Young, Compilers, Los Alamos National Laboratory report LA-8874-PR, p. 15 (1981).
13. B. B. Back, O. Hawsen, H. C. Britt, and J. D. Garrett, "Fission of Doubly Even Actinide Nuclei Induced by Direct Reactions," Phys. Rev. C9, 1924 (1974).
14. G. Haouat, Ch. Lagrange, J. Lachkar, J. Jary, Y. Patin, and J. Sigaud, "Fast Neutron Scattering Cross Sections for Actinide Nuclei," in Proceedings of the International Conference on Nuclear Cross Sections for Technology, NBS Special Publication 594, p. 672 (1980).
15. D. G. Madland and J. R. Nix, Trans. Am. Nucl. Soc. 32, 726 (1979).
16. D. G. Madland and J. R. Nix, Bull. Am. Phys. Soc. 24, 885 (1979).

17. D. G. Madland and J. R. Nix, Proceedings of the International Conference on Nuclear Cross Sections for Technology, Knoxville, Tenn., Oct. 22-26, 1979 (NBS Special Publication 594, Washington, 1980) p. 788.
18. D. G. Madland and J. R. Nix, Proceedings of the International Conference on Nuclear Physics, Berkeley, Calif., Aug. 24-30, 1980 (to be published).
19. D. G. Madland, Proceedings of the Workshop on Evaluation Methods and Procedures, BNL, Upton, New York, Sept. 22-25, 1980 (to be published).
20. D. G. Madland, Trans. Am. Nucl. Soc. 38, 649 (1981).
21. M. Abramowitz and I. A. Stegun, Eds., Handbook of Mathematical Functions, National Bureau of Standards, Washington, D.C. (1964), pp. 227-266.
22. J. P. Unik, J. E. Gindler, L. E. Glendenin, K. F. Flynn, A. Gorski, and R. K. Sjoblom, Proceedings of the Third IAEA Symposium on the Physics and Chemistry of Fission, Rochester, New York, 1973 (IAEA, Vienna, 1974) Vol. II, p. 19.
23. A. H. Wapstra and K. Bos, "The 1977 Atomic Mass Evaluation," Atomic Data Nucl. Data Tables 19, 177 (1977).
24. W. D. Myers, Droplet Model of Atomic Nuclei, (IFI/Plenum Data Co., New York, 1977).
25. J. Grundl and C. Eisenhauer, Proceedings of a Consultants' Meeting on Integral Cross Section Measurements in Standard Neutron Fields for Reactor Dosimetry, Vienna, November 15-19, 1976 (IAEA, Vienna, 1978) Vol. I, p. 53.
26. M. R. Bhat, "Evaluation of ^{235}U Neutron Cross Section and Gamma Ray Production Data for ENDF/B-V," National Nuclear Data Center report BNL-NCS-51184 (ENDF-248) p. 48, 1980 (Brookhaven National Laboratory, March, 1980).
27. ENDF-202, Cross Section Evaluation Working Group Benchmark Specifications, Brookhaven National Laboratory report BNL 19202 (ENDF-202) 1974.
28. D. G. Madland, "Calculation of Excited State Cross Sections for Actinide Nuclei" in "Applied Nuclear Data Research and Development January 1-March 31, 1981," Los Alamos National Laboratory report LA-8874-PR, p. 16 (1981).
29. G. E. Hansen and H. C. Paxton, "Fast Critical Specifications in Benchmark Format," Los Alamos National Laboratory internal memorandum no. Q-14-79-314, to R. J. LaBauve, 18 Oct. 1979.
30. R. D. O'Dell, F. W. Brinkley, Jr., and D. R. Marr, "ONEDANT, A Code Package for One-Dimensional, Diffusion-Accelerated, Neutral-Particle Transport," Los Alamos National Laboratory report (to be published).
31. R. E. MacFarlane, R. J. Barrett, D. W. Muir, and R. M. Boicourt, "The NJOY Nuclear Data Processing System: User's Manual," Los Alamos Scientific Laboratory report LA-7584-MS (ENDF-272) (1978).

32. D. Garber, Ed., "Data Formats and Procedures for the ENDF Neutron Cross Section Library," Brookhaven National Laboratory report BNL 50274 (1976).
33. W. B. Wilson, T. R. England, R. J. LaBauve, and R. M. Boicourt, "The TOAFEW-V, Multigroup Cross-Section Collapsing Code and Library of 154-Group Processed ENDF/B-V Fission-Product and Actinide Cross Sections," prepared for the Electric Power Research Institute, May 1981. [See Los Alamos Scientific Laboratory report LA-7174-MS, 1978, for similar report using ENDF/B-IV fission products; the LWR weighting function is also described in this document].
34. T. R. England, W. B. Wilson, and R. E. Schenter, "Fission-Product and Actinide Data: Summary of Major Data in ENDF/B-V," Los Alamos National Laboratory report (in preparation).
35. J. Grundl and C. Eisenhauer, "Fission Rate Measurements for Materials Neutron Dosimetry in Reactor Environments," Proceedings of the First ASTM-EURATOM Symposium on Reactor Dosimetry, Pittin (Holland), 1975.
36. C. M. Eisenhauer, private communication (excerpt from NBS report in preparation, "Compendium of Benchmark and Test Region Neutron Fields for Pressure Vessel Irradiation Surveillance." This excerpt from a section titled "Standard Neutron Field Entry - Fission Neutron Spectra").
37. D. M. Gilliam, "Integral Measurement Results in Standard Fields," Proceedings International Symposium on Neutron Standards and Applications, NBS Special Publ. 493, U.S. Dept. of Commerce, Washington, D.C., (March 1977).
38. B. A. Magurno, "Status of the Dosimetry File for ENDF/B-V," Proc. Advisory Group Mtg. Nuclear Data for Reactor Dosimetry, INDC(nds)-103M, p. 1, Nuclear Data Section, Int. Atomic Energy Agency (1979).
39. R. E. Seamon, "Cross Sections for Monte Carlo Calculations-X-6 Activity Report," Los Alamos Scientific Laboratory report LA-8232-PR (February 1980.).
40. W. Mannhart, "Progress in Integral Data and Their Accuracy: Average Neutron Cross Sections in the Californium-252 Benchmark Field," Nucl. Sci. Eng. Vol. 77 (1), p. 40 (1981).
41. G. Winkler, V. Spiegel, C. Eisenhauer, D. Smith, "Measurement of the Average Activation Cross Section for the Reaction $^{63}\text{Cu}(n, \alpha)^{60}\text{Co}$ in the Spontaneous Fission Neutron Field of Californium-252," Progress Report to the International Nuclear Data Committee, INDC(AUS)-006/G (May 1981).
42. R. E. MacFarlane, "Energy Balance of ENDF/B-V," Trans. Am. Nuc. Soc. 33, 681 (1979).
43. Evaluated Nuclear Data Library, Version 5 (ENDF/B-V), maintained and distributed by the Brookhaven National Laboratory. (Most of the experimental decay energies in this library were evaluated at INEL; summary data for all nuclides are available from Los Alamos as part of a document being prepared for publication.)

44. Tadashi Yoshida and Tyuzo Nakasima, "Decay Heat Calculation based on Theoretical Estimation of Average Beta- and Gamma-Energies Released from Short-Lived Fission Products," J. Nucl. Sci. and Tech. 18, No. 6, 393 (June 1981).
45. A. Tobias and B. S. J. Davies, "UKFPDD-2: A Revised Fission Product Decay Data File in ENDF/B-IV Format," Central Electricity Generating Board report RD/B.N4942 (November 1980).
46. Evaluated Nuclear Data Library ENDF/B-IV (see Ref. 44).
47. J. K. Dickens, T. A. Love, J. W. McConnell, and R. W. Peelle, Nucl. Sci. Eng. 74, 106 (1980).
48. J. K. Dickens, T. A. Love, J. W. McConnell, and R. W. Peelle, Oak Ridge National Laboratory report ORNL/NUREG-34 (April 1978). [Also, Dickens, T. A. Love, J. W. McConnell, and R. W. Peelle, Nucl. Sci. Eng. 78, 126 (1981)].
49. E. T. Journey, P. J. Bendt, and T. R. England, "Fission Product Gamma Spectra," Los Alamos Scientific Laboratory report LA-7620-MS (January 1979).
50. R. J. LaBauve, T. R. England, D. C. George, and M. G. Stamatelatos, "The Application of a Library of Processed ENDF/B-IV Fission-Product Aggregate Decay Data in the Calculation of Decay-Energy Spectra," Los Alamos Scientific Laboratory report LA-7483-MS (September 1978).
51. T. R. England, R. Wilczynski, and N. L. Whittemore, "CINDER-7: An Interim Report for Users," Los Alamos Scientific Laboratory report LA-5885 (April 1976). [CINDER-10, the version used in this report is unpublished; it is described in "Applied Nuclear Data Research and Development Jan. 1- Mar. 31, 1976," Los Alamos Scientific Laboratory report LA-6472-PR, (1976) p. 60, and in "Applied Nuclear Data Research and Development Oct. 1-Dec. 31, 1975," Los Alamos Scientific Laboratory report LA-6266-PR (1976) p. 13.]
52. R. J. LaBauve and T. R. England, "Integral Data Testing of ENDF/B Fission Product Data," report presented to CSEWG meeting, Brookhaven National Laboratory, May 1981 (LA-UR-81-1417). This information transmitted in personal communication with R. E. Schenter, Hanford Eng. Dev. Lab., and is accessible through T. R. England, Los Alamos.
53. J. C. Hardy, L. C. Carraz, B. Jonson, and P. G. Hansen, Phys. Letters 71B, 307 (1977).
54. F. Schmittroth, "Theoretical Estimates of Decay Information for 'Non-Experimental Nuclides,'" Proc. of the BNL Workshop on Evaluation Methods and Procedures for Applied Nuclear Data, Sept. 22-25, 1980
55. T. Yamamoto, M. Akiyama, Z. Matumoto, and R. Nakasima, Japanese Atomic Energy Research Institute report JAERI-M-9357 [NEANDC(J)-72N, INDC(JAP)-59/L] (February 1981).
56. F. M. Mann, C. Dunn, and R. W. Schenter, "Beta Decay Properties from a Statistical Model" (contributed paper for the Am. Nucl. Soc. Meeting, San Francisco, Nov. 1981).

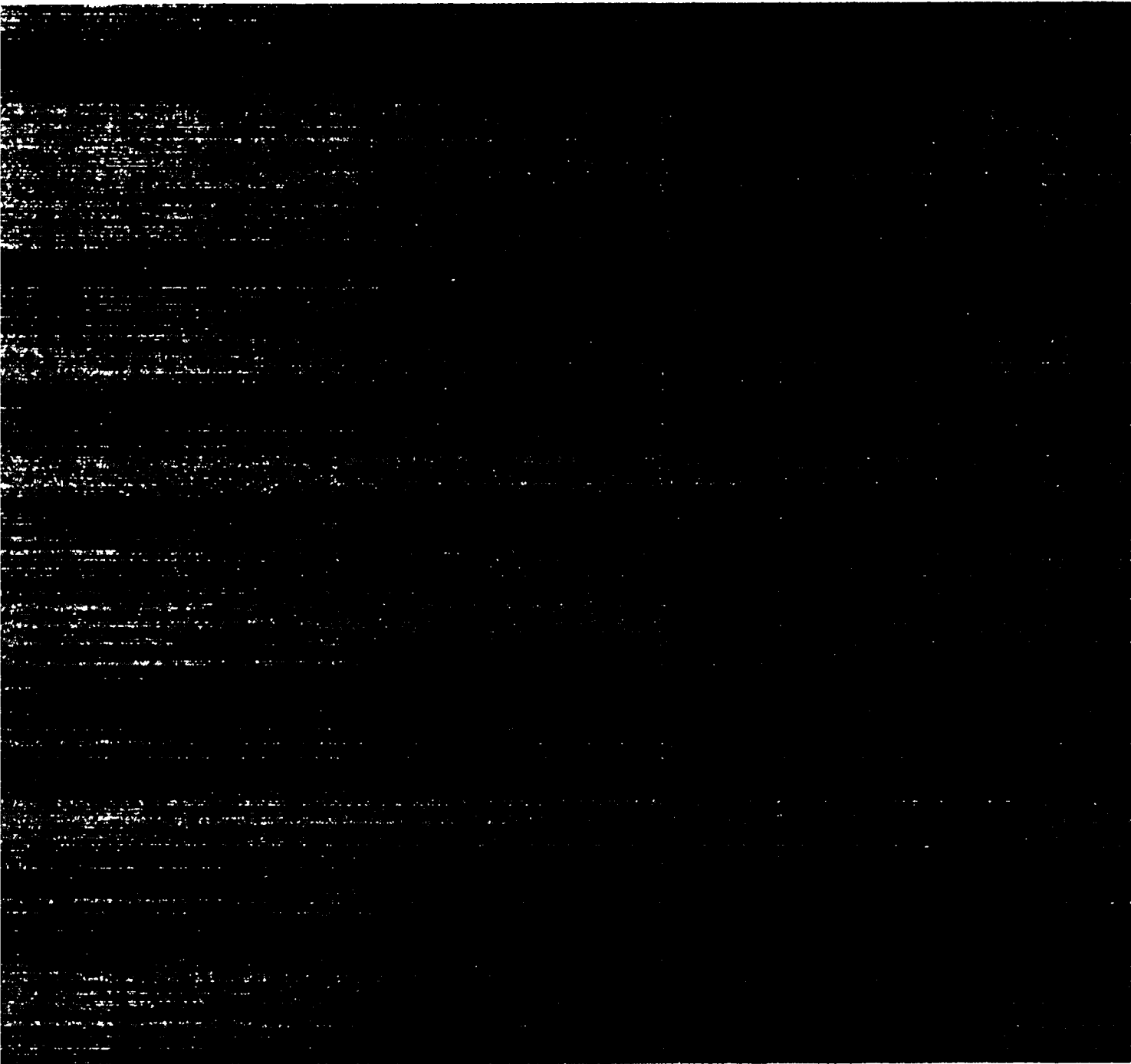
57. R. J. LaBauve, D. C. George, T. R. England, "Integral Data Testing of ENDF/B Fission-Product Data," in "Applied Nuclear Data Research and Development January 1-March 31, 1981," Los Alamos National Laboratory report LA-8874-PR, p. 37 (1981).
58. Fission-Product Decay Library of the Evaluated Nuclear Data File, Version V (ENDF/B-IV). [Available from and maintained by the National Nuclear Data Center (NNDC) at Brookhaven National Laboratory.]
59. Fission-Product Decay Library of the Evaluated Nuclear Data File, Version V (ENDF/B-V). [Available from and maintained by the National Nuclear Data Center (NDC) at Brookhaven National Laboratory.]
60. J. K. Dickens, T. A. Love, J. W. McConnell, J. F. Emery, K. J. Northcutt, R. W. Peelle, and H. Weaver, "Delayed Beta- and Gamma-Ray Production Due to Thermal-Neutron Fission of ^{235}U , Spectral Distributions for Times After Fission Between 2 and 14 000 sec: Tabular and Graphical Data," Oak Ridge National Laboratory report NUREG/CR-0162, ORNL/NUREG-39 (August 1978).
61. J. K. Dickens, T. R. England, T. A. Love, J. W. McConnell, J. F. Emery, K. J. Northcutt, and R. W. Peelle, "Delayed Beta- and Gamma-Ray Production Due to Thermal-Neutron Fission of ^{239}Pu : Tabular and Graphical Spectral Distributions from Times After Fission Between 2 and 14 000 sec," Oak Ridge National Laboratory report NUREG/CR-1171, ORNL/NUREG-66 (January 1980).
62. E. T. Journey, P. J. Bendt, and T. R. England, "Fission Product Gamma Spectra," Los Alamos Scientific Laboratory report LA-7620-MS (January 1979).
63. T. Yamamoto, M. Akiyama, Z. Matumoto, and R. Nakasima, Japanese Atomic Energy Research Institute report JAERI-M-9357 [NEANDC(J)-72N, INDC(jap)-59/L] (February 1981).
64. T. R. England, W. B. Wilson, and R. E. Schenter, "ENDF/B-V MOD "O" Summary Data for Fission Products and Actinides," report presented to CSEWG meeting Brookhaven National Laboratory, May 1981 (LA-UR-81-1418).
65. R. T. Perry and W. B. Wilson, "Neutron Production from (α ,n) Reactions and Spontaneous Fission in ThO_2 , UO_2 , and $(\text{U,Pu})\text{O}_2$ Fuels," Los Alamos National Laboratory report LA-8869-MS (June 1981).
66. J. K. Bair and H. B. Willard, "Level Structure in Ne^{22} and Si^{30} from the Reactions $^{18}\text{O}(\alpha,n)\text{Ne}^{21}$ and $\text{Mg}^{26}(\alpha,n)\text{Si}^{29}$," Phys. Rev. 128, 299 (1962).
67. J. K. Bair and F. X. Haas, "Total Neutron Yield from the Reactions $^{13}\text{C}(\alpha,n)^{16}\text{O}$ and $^{17,18}\text{O}(\alpha,n)^{20,21}\text{Ne}$," Phys. Rev. C7, 1356 (1973).
68. J. K. Bair and J. Gomez del Campo, "Neutron Yields from Alpha-Particle Bombardment," Nucl. Sci. Eng. 71, 18 (1979).
69. L. F. Hansen, J. D. Anderson, J. W. McClure, B. A. Pohl, M. L. Stlts, J. J. Wesolowski, and C. Wong, "The (α ,n) Cross Sections on ^{17}O and ^{18}O Between 5 and 12.5 MeV," Nucl. Phys. A98, 25 (1967).

70. M. Balakrishnan, S. Kailas, and M. K. Mehta, "A Study of the Reaction $^{19}\text{F}(\alpha, n)^{22}\text{Na}$ in the Bombarding Energy Range 2.6 to 5.1 MeV," *Pramana* 10, 329 (1978).
71. W. B. Wilson, J. E. Stewart, and R. T. Perry, "The $^{19}\text{F}(\alpha, n)$ Neutron Production from the Decay of U Nuclides in UF_6 ," in "Applied Nuclear Data Research and Development, October 1 - December 31, 1980," Los Alamos National Laboratory report LA-8757-PR (March 1981).
72. W. H. Bragg and R. Kleeman, "On the Alpha Particles of Radium and Their Loss of Range in Passing Through Various Atoms and Molecules," *Phil. Mag.* 10, 318 (19).

Printed in the United States of America
 Available from
 National Technical Information Service
 U.S. Department of Commerce
 5285 Port Royal Road
 Springfield, VA 22161
 Microfilm \$3.50 (A01)

Page Range	Domestic Price	NTIS Price Code	Page Range	Domestic Price	NTIS Price Code	Page Range	Domestic Price	NTIS Price Code	Page Range	Domestic Price	NTIS Price Code
1-25	\$ 5.00	A02	151-175	\$11.00	A08	301-325	\$17.00	A14	451-475	\$23.00	A20
26-50	6.00	A03	176-200	12.00	A09	326-350	18.00	A15	476-500	24.00	A21
51-75	7.00	A04	201-225	13.00	A10	351-375	19.00	A16	501-525	25.00	A22
76-100	8.00	A05	226-250	14.00	A11	376-400	20.00	A17	526-550	26.00	A23
101-125	9.00	A06	251-275	15.00	A12	401-425	21.00	A18	551-575	27.00	A24
126-150	10.00	A07	276-300	16.00	A13	426-450	22.00	A19	576-600	28.00	A25
									601-up		A99

(Add \$1.00 for each additional 25-page increment or portion thereof from 601 pages up)



Los Alamos